Bulletin of Electrical Engineering and Informatics
Vol. 15, No. 2, April 2026, pp. 1590∼1628
ISSN: 2302-9285, DOI: 10.11591/eei.v15i2.10914

A modified transfer function for frequency sampling filters: theory, design, and applications

Serhii Rybka[1], Ivan Varava[2]
[1]G.E. Pukhov Institute for Modelling in Energy Engineering, Kyiv, Ukraine
[2]Department of Software Engineering in Energy, Educational and Scientific Institute of Nuclear and Thermal Energy, National Technical University of Ukraine "Igor Sikorsky Kyiv Polytechnic Institute", Kyiv, Ukraine

Article Info

Article history:

Received Jun 25, 2025
Revised Dec 10, 2025
Accepted Feb 22, 2026

Keywords:

Digital filter
Filter bank
Finite impulse response
Linear-phase response
Multiband filter
Spectrum analyzer

ABSTRACT

The article is devoted to frequency sampling filters (FSF). FSFs are highly efficient linear-phase digital filters that can be significantly more computationally efficient than Parks–McClellan FIR filters. FSFs are well-suited for implementing filter banks, which can be used to construct high-performance spectrum analyzers. Although these filters have been known for a long time, they have not been widely adopted despite their efficiency. This article presents the authors' perspective on the reasons behind the limited use of FSFs. A new original method for forming the transfer function (TF) of FSFs using an ideal analog prototype is proposed. The proposed method fundamentally differs from the long-established classical approach. The TF of an analog filter that meets the requirements of absolute linearity in the phase response (PR) was considered. The bilinear z-transform method was applied to this ideal TF. By applying L'Hôpital's rule, an analytical expression for determining the weighting coefficients of the resulting TF was obtained. The article presents examples of calculated FSFs and a filter bank based on them. Tables of the optimized weighting coefficients and plots of their attenuation characteristics are provided. An improved block diagram of the FSF is also presented. The characteristics of the classical FSF TF and the proposed (alternative) FSF TF are analyzed and compared to determine their advantages and disadvantages.

Corresponding Author:

Serhii Rybka
G.E. Pukhov Institute for Modelling in Energy Engineering
Kyiv, Ukraine
Email: ars09@ukr.net

1. INTRODUCTION

Frequency sampling filters (FSF) allow for the design of high-performance low-pass, band-pass, and high-pass FIR filters. They have been known since the late 1960s [1]. However, as of today, FSF are not widely used [2]. In our opinion, the lmited application is due to a number of unresolved issues, namely:

a. The lack of publicly available FSF design technology that enables simultaneous control of passband ripple and guaranteed attenuation in the stopband while achieving the specified cutoff frequencies;
b. The approximation problem in filter design belongs to the class of nonlinear programming problems. Therefore, it cannot be solved in a straightforward manner. To solve it successfully, it is necessary to be able to use a good initial solution. However, there is no generally accepted criterion for determining whether an initial solution is suitable for successfully solving the FSF approximation problem;

c. There is no publicly available analytical formulation of a clear criterion for evaluating the achievement of the best optimal solution to the FSF approximation problem.

d. The issue of achieving phase linearity in filters implemented by the frequency sampling method has been insufficiently addressed in the literature.

The existing FSF design technologies [3]–[12] do not address all of the aforementioned issues. Therefore, the further development of FSF design technology remains a relevant and important research topic.

This article presents the results of a study aimed at finding new effective solutions for the synthesis of digital filter banks with a linear phase response (PR). During the research, a modified transfer function (TF) for FSFs was obtained, featuring new properties.

It is well known that the synthesis of digital filters often involves design methods based on physically realizable analog prototypes, followed by the transformation of their TF into the z-domain [1], [13]. These methods are attractive because they enable the use of a powerful, well-established mathematical arsenal developed for approximating FR in the synthesis of analog electrical circuits [14]. Such studies require additional effort to gain a deep understanding of the mathematical framework used in analog filter design. It is likely that the reluctance or unpreparedness to master this knowledge discourages many researchers. However, this knowledge allows for the development and application of remarkable new results in digital filter design. Especially valuable is the understanding of how to solve the most challenging aspect of filter design - the approximation problem. In the era of "digitalization" of scientific discourse on filter design, it would be unwise to disregard the accumulated knowledge and refined mathematical tools of analog filter design or to consider research methods based on this foundation as marginal.

For the study, an analog prototype [15], [16] constructed using cascaded LC-resonators was selected. The resonators are connected in parallel, and taps are taken from their midpoints to form the filter's output signal. This structure is of particular interest because all the resonators contribute to the formation of the output signals at all individual outputs of the filter bank, making it highly efficient. The more resonators are used, the better the FR that can be achieved. Ideally, the number of LC-resonators should approach infinity. In this case, the filter exhibits an absolutely linear phase. Obviously, such a TF cannot be realized in an analog element based. However, it turns out that this ideal TF can be implemented in a digital element based. To transform the ideal TF of the multiband filter with linear phase, the bilinear z-transform was used.

Thus, a new original approach was implemented. Traditionally, a physically realizable analog prototype is used. In the generally accepted approach [1], [13], [14] constraints are introduced into the TF, which lead to distortions in the FR, primarily in the PR. As a result, the TF becomes non-ideal.

As a result of the study, a modified (alternative) TF for a FIR FSF with real coefficients and a linear PR was obtained, featuring new useful properties. This TF is subsequently used in a direct method for FSF synthesis. The methods for solving the approximation problem of the analog prototype [16] were studied and successfully applied to the approximation of digital filters. A design technology for FSFs was developed, which, through the optimization of weighting coefficients in the transition bands, allows suppression of the Gibbs phenomenon, control of ripples in both the passband and stopband, and smooth tuning of cutoff frequencies. The coefficient tables and attenuation characteristics plots presented in the article demonstrate examples of optimal solutions to the approximation problem for bandpass FSFs and filter banks based on the obtained modified (alternative) TF.

For comparison, four types of classical FSF TF and an alternative FSF TF were considered. Their magnitude-frequency, phase-frequency, and impulse responses (IR), as well as group-delay characteristics and pole-zero plots, were calculated and analyzed. The obtained results are presented in the corresponding figures.

This article is an initial material on the technology of designing FSF banks using the obtained TF of FSFs with real coefficients. It aims to provide a theoretical overview and examine the main properties of the modified FSF TF. Further discussion of the research results related to the developed FSF design technology will be presented in future articles.

2. ANALYSIS OF THE TRANSFER FUNCTION OF A MULTIBAND ELECTRICAL PROTOTYPE FILTER

In the works of Babkova and Beletsky [15] and Babkova [16] substantiated the possibilities of synthesizing a multiband electrical filter in the form of a transversal structure of an LC-multipole network (one input and l-outputs), which has a number of advantages. All elements of the multipole take part in the formation

of the FR of each of the outputs. As a result, a significant reduction in the number of elements is achieved compared to a filter bank implemented as a set of individual electrical filters. Based on the proposed structure it is possible to implement any required FR shape and a PR close to linear. In this case, the values of the group delay time will be almost equal for each of the l-outputs of the multiband filter (Figure 1).

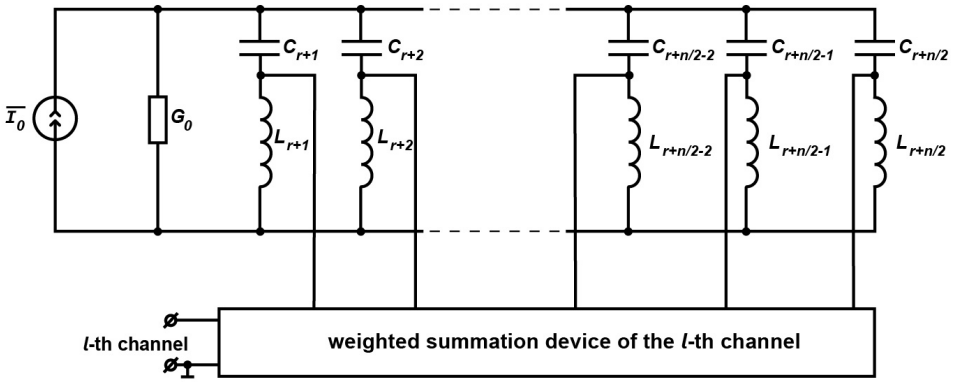

Figure 1. Schematic of a multiband electrical filter

The TF of a physically realizable multiband electrical filter (Figure 1) for the l-th output can be written in the following form [15], [16]:

$$T_l(s) = \frac{\overline{U}_{lout}}{\overline{I}_0} = \frac{\sum_{k=r+1}^{r+n/2}(a_k \frac{s^2}{s^2+\omega_k^2})}{1+\sum_{k=r+1}^{r+n/2}(b_k \frac{s}{s^2+\omega_k^2})}$$

here $s = \alpha + j\omega$: Laplace operator.

Let us consider in more detail the theoretical calculations underlying the synthesis of the structure in the form of a transversal structure of an LC-multipole (Figure 1). The TF for the l-th output of a multiband electrical filter can be represented as a rational fraction (1) [17]:

$$T_l(s) = \frac{A_{0l}s^n + A_{2l}s^{n-2} + A_{4l}s^{n-4} + \cdots}{s^\mu + B_1 s^{\mu-1} + B_2 s^{\mu-2} + \cdots + B_\mu} = \frac{W_l(s)}{V(s)}, \tag{1}$$

where $n \leq \mu$;
$W_l(s)$: even or odd polynomial with real coefficients, which is the different for each output;
$V(s)$: Hurwitz polynomial, which is the same for the TF of any of the outputs of the multiband electric filter.

If the numerator and denominator of function (1) are divided by the even part of the Hurwitz polynomial (let n be an even number), then expression (1) is transformed to the form:

$$T_l(s) = \frac{\frac{2W_l(s)}{V(s)+V(-s)}}{1+\frac{V(s)-V(-s)}{V(s)+V(-s)}}, \tag{2}$$

here:
$V(-s)$: conjugate Hurwitz polynomial;
$\frac{1}{2}(V(s)+V(-s))$: even part of the Hurwitz polynomial;
$\frac{1}{2}(V(s)-V(-s))$: odd part of the Hurwitz polynomial.
If $W_l(s)$ – is an even polynomial, then the numerator (2) in the general case can be represented as [15]:

$$\frac{2W_l(s)}{V(s)+V(-s)} = \sum_{k=1}^{n/2} a_k \frac{s^2}{s^2+\omega_k^2}, \tag{3}$$

here ω_k: resonant frequency.

Let us make an important assumption, which boils down to the requirement of approximating the linear PR over the entire operating frequency band of the filter. It is known [17], [18] that the PR of the filter in the passband is determined only by the Hurwitz polynomial $V(s)$, therefore, with the required accuracy (the accuracy is determined by the permissible phase nonlinearity) in this band, it is necessary to fulfill the equality [19]-[21]:

$$arctan\frac{1}{j}\frac{V(s)-V(-s)}{V(s)+V(-s)} \cong \tau\pi, \tag{4}$$

here τ: slope of the phase-frequency response.
From (4) we find:

$$\frac{\frac{V(s)}{V(-s)}-1}{\frac{V(s)}{V(-s)}+1} \cong jtan\tau\omega.$$

Hence:

$$\frac{V(s)}{V(-s)} \cong \frac{1+jtan\tau\omega}{1-jtan\tau\omega}.$$

Because $jtan\tau\omega = tanhs$ [18], we write down:

$$\frac{V(s)}{V(-s)} \cong \frac{1+jtan\tau\omega}{1-jtan\tau\omega} = \frac{cosh\tau s+sinh\tau s}{cosh\tau s-sinh\tau s}. \tag{5}$$

Based on (5), we can conclude that in order to satisfy the requirement of ensuring the specified linearity of the PR of the filter, the Hurwitz polynomial $V(s)$ must reproduce the meromorphic function $cosh\tau s+sinh\tau s$ with sufficient accuracy. It is known [22] that:

$$cosh\tau s + sinh\tau s = e^{\tau s}. \tag{6}$$

Therefore, the denominator of the ideal TF, which is subject to approximation, has the form: $V(s) = e^{\tau s}$. The function $e^{\tau s}$ must be approximated by the Hurwitz polynomial.

It is evident that, in order to achieve absolute linearity of the filter's PR, the following condition must be satisfied: the coefficients of the polynomial in the denominator of the filter TF must correspond to the coefficients of the Hurwitz polynomial that approximates function $e^{\tau s}$ (6), when its order approaches infinity.

The limiting condition of the linearity of the filter's PR, let us call it so, is impracticable when implemented on an analog basis. The condition, when the order of the polynomial in the denominator approaches infinity, corresponds to an infinite number of elements in an electric circuit that implements a TF with such a denominator (6). Therefore, in practice, they resort to limiting the dimension of the denominator polynomial [19], [20], which leads to distortions of the PR of the analog filter. As will be shown below, the boundary condition of linearity of the PR is easily satisfied for FSF. This is a remarkable property of FSF.

The PR of the filter in the passband is determined only by the Hurwitz polynomial $V(s)$, and the attenuation response is determined by both the $V(s)$ polynomial and the $W_l(s)$ polynomial. When the limiting condition of linearity of the PR of the filter is fulfilled, the attenuation characteristic will be determined only by the polynomial of the numerator $|e^{\tau s}| = 1$.
Then the TF of the filter with a linear PR will have the form:

$$T_l(s) = W_l(s)e^{-\tau s}. \tag{7}$$

In this case, the problem of approximation is reduced to finding the value of the coefficients of the even or odd polynomial $W_l(s)$, the modulus of which will more accurately approximate the given attenuation characteristic in the passband and provide the greater the value of the stopband attenuation, the higher the degree of this polynomial. However, the solution of the problem of approximation of the TF of the form (7) is rather difficult. To implement the specified requirements for the filter, the TF of the form (7) requires the use of high-order polynomials.

Based on the above considerations, in order to theoretically fulfill the limiting condition for linearity of the PR of the filter, it is necessary to replace:

$$V(s) = cosh\tau s + sinh\tau s; V(-s) = cosh\tau s - sinh\tau s.$$

Then:

$$V(s) + V(-s) = 2cosh\tau s; V(s) - V(-s) = 2sinh\tau s.$$

Hence:

$$1 + \frac{V(s) - V(-s)}{V(s) + V(-s)} = 1 + tanh\tau s = \frac{cosh\tau s + sinh\tau s}{cosh\tau s} = \frac{e^{\tau s}}{cosh\tau s}. \tag{8}$$

If the polynomial of the denominator of the TF of general form is formed using the finite sum of the expansion of the hyperbolic function $cosh\tau s$ in an infinite series, then using the relation given in [23]:

$$cosh\tau s = -\frac{1}{\pi\omega} + \frac{2}{\pi}\sum_{k=0}^{\mu/2}\Big(\frac{\omega}{\omega^2 - \omega_k^2}\Big),$$

where for convenience it is accepted $\tau = \pi$.
Passing to a finite sum and keeping a finite number of terms in the expansion, we find:

$$cot\omega\pi \cong \frac{2}{\pi}\sum_{k=0}^{\mu/2}\Big(\frac{\omega}{\omega^2 - \omega_k^2}\Big).$$

However, solving the problem posed ultimately to go to a digital elemental basis, it makes no sense to go to a finite number of terms in the denominator of the TF and thereby introduce distortions in the PR of the implemented filter.
Function (2), taking into account (3) and (8), can be written:

$$\begin{aligned} T_l(s) &= \sum_{k=1}^{n/2}\Big(a_k\frac{s^2}{s^2 + \omega_k^2}\Big)sinh\tau s e^{-\tau s}, \\ T_l(s) &= \sum_{k=1}^{n/2}\Big(a_k\frac{s^2}{s^2 + \omega_k^2}\Big)cosh\tau s e^{-\tau s}. \end{aligned} \tag{9}$$

It is known [18], [20] that:

$$sinh\tau s = \frac{e^{\tau s} - e^{-\tau s}}{2}; cosh\tau s = \frac{e^{\tau s} + e^{-\tau s}}{2}. \tag{10}$$

Taking into account (10), function (9) can be represented in the following form:

$$T_l(s) = \sum_{k=1}^{n/2}\Big(a_k^*\frac{s^2}{s^2 + \omega_k^2}\Big)(1 \pm e^{-2\tau s}). \tag{11}$$

In this case, the approximation problem is extremely simplified and is reduced to finding only the coefficients of the numerator a_k^*. Thus, the number of required coefficients is reduced by at least half (since the order of the numerator is less than the order of the denominator (1)). Obviously, the larger the number of terms a polynomial has, the more stringent conditions imposed on the FR can be satisfied. Using the TF (11), it is theoretically possible to fulfill any given requirements for the FR of multiband electric filter with a linear PR in the entire operating frequency band. The simplest analysis of the components of the function (11) proves the absolute linearity of the dependence of the value of its argument on frequency. It is easy to see that the polynomial $\sum_{k=1}^{n/2}\Big(a_k^*\frac{s^2}{s^2+\omega_k^2}\Big)$ has a zero complex component (since $s^2 = -\omega^2$ at $\alpha = 0$), therefore has a

zero-argument value. Factor $(1 \pm e^{-2\tau s})$ also has a linear dependence of the argument on frequency. Obviously, the total PR of the ideal filter implemented using (11) will be linear. The formulation of the linearity condition for the PR makes it possible to achieve the potential for simplifying the filter TF.

The limitations arising in the implementation of filters in an analog basis based on the TF (11) (the number of circuit elements tends to infinity) can be overcome when designing digital filters if we use the considered TF as an ideal analog prototype for obtaining a system function of the general form of a multiband digital filter. In the future, it can be used in the method of direct synthesis of digital filters. Knowing the properties of the transformation into the z-plane of transcendental functions, it seems possible to abandon the solution of the problem of approximating the denominator of the TF for each of the outputs of the multiband filter. It leads to a significant reduction in the number of arithmetic operations in the digital element basis when fulfilling the specified requirements for the FR, to linear form PR for all outputs of the multiband digital filter and ensuring its stability.

3. CONVERSION OF THE TRANSFER FUNCTION OF AN IDEAL ANALOG MULTIBAND FILTER PROTOTYPE FROM THE S-PLANE TO THE Z-PLANE

We transform the TF (11) of the ideal analog prototype from the s-plane to the z-plane. Taking into account that the part of the TF (11), determined by the expression $(1 \pm e^{-2\tau s})$, is common for all outputs of the multiband filter, then $T_l(s)$ can be written as the product of two functions:

$$T_l(s) = T_{1l}(s) T_2(s), \tag{12}$$

here

$$T_{1l}(s) = \sum_{k=1}^{n/2} \left(a_k^* \frac{s^2}{s^2 + \omega_k^2} \right),$$

$$T_2(s) = 1 - e^{2\tau s}.$$

For clarity, Figure 2 presents the magnitude responses of the TF $T_l(s)$ in its general form and its components. Specifically, Figure 2(a) shows the magnitude of $T_{1l}(s)$, Figure 2(b) shows the magnitude of $T_2(s)$, and Figure 2(c) shows the magnitude of $T_l(s)$.

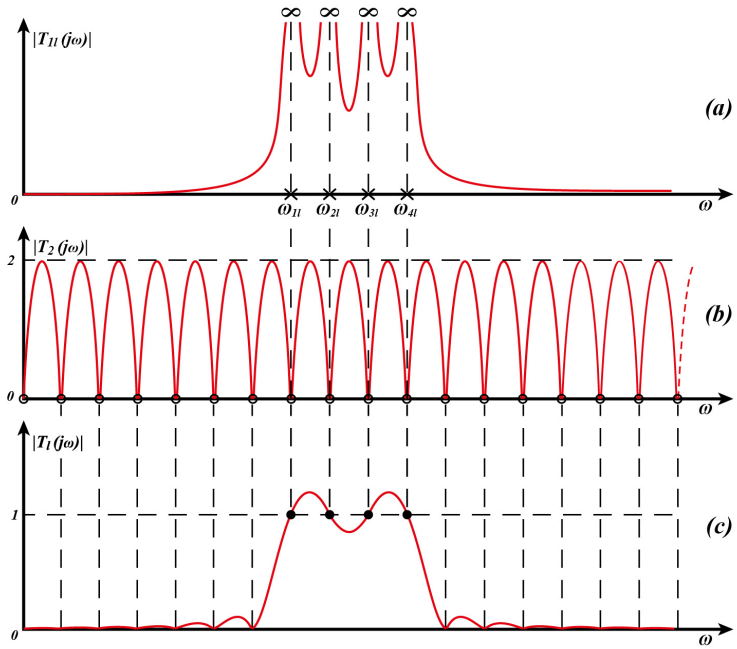

Figure 2. Graphs of the magnitude of the TF: (a) $T_{1l}(s)$; (b) $T_2(s)$; and (c) $T_l(s)$ of the general form (12)

To transform $T_{1l}(s)$ from the s-plane to the z-plane, we will use the bilinear z-transform method [1]. The method provides a one-to-one, but not ideal, mapping of the s-plane to the z-plane, while maintaining the order of the TF. The deformation of the frequency scale in this case is not critical, since the transformation aims to obtain the general form of the TF in the z-plane for further use in the direct method of digital filter synthesis. The transformation procedure of the TF $T_l(s)$ (12) is shown below. First, let's change the variable [1]:

$$s \to \frac{2}{T}\frac{1-z^{-1}}{1+z^{-1}},$$

here $z = exp(j\Omega)$;
Ω: digital frequency.
Then:

$$\sum_{kl=1}^{nl} A_{kl}^0 \frac{\left(\frac{2}{T}\frac{1-z^{-1}}{1+z^{-1}}\right)^2}{\left(\frac{2}{T}\frac{1-z^{-1}}{1+z^{-1}}\right)^2 + \omega_{kl}^2} = (1-z^{-1})^2 \sum_{kl=1}^{nl} \frac{A_{kl}^0}{(1-z^{-1})^2 + (\frac{\omega_{kl}T}{2})^2(1+z^{-1})^2} =$$

$$= (1-z^{-1})^2 \sum_{kl=1}^{nl} \frac{A_{kl}^*}{1+(2\frac{k-1}{k+1})z^{-1}+z^{-2}} = (1-z^{-1})^2 \sum_{kl=1}^{nl} \frac{A_{kl}^*}{1+b_{1kl}z^{-1}+z^{-2}}, \tag{13}$$

here $A_{kl}^* = \frac{A_{kl}^0}{1+k}$; $k = \left(\frac{\omega_{kl}T}{2}\right)^2$; $b_{1kl} = 2\frac{k-1}{k+1}$.
It is known [1] that analog frequency ω and digital Ω with bilinear z-transform are related by the ratio:

$$\omega = \frac{2}{T}tan(\frac{\Omega T}{2}).$$

Obviously:

$$\omega_{kl} = \frac{2}{T}tan(\frac{\Omega_{kl}T}{2}).$$

Therefore, taking into account (13):

$$k = tan^2(\frac{\Omega_{kl}T}{2}). \tag{14}$$

Let's enter the normalized digital frequency:

$$x = \Omega T \to x_{kl} = \Omega_{kl}T, \tag{15}$$

here x_{kl}: fixed values of the normalized digital frequency at specific points; $x \in [0, \pi]$.
Referring to the notation adopted in (13) and to expressions (14), (15), we write the equality:

$$b_{1kl} = 2\frac{k-1}{k+1} = -2cos(x_{kl}).$$

The obtained result confirms that the TF of the analog prototype (11) is theoretically correct. The polynomial in function (13), after being transformed into the z-plane, generates the required zeros. It has been analytically proven that the feedback coefficient b_{1k} is determined as the root of a second-order equation. Therefore, we can write:

$$T_{1l}(s) \to H_{1l}(z),$$

$$H_{1l}(z) = (1-z^{-1})^2 \sum_{kl=1}^{nl} \Big(\frac{A_{kl}^*}{1+b_{1kl}z^{-1}+z^{-2}}\Big). \tag{16}$$

Now we transform the second part of the TF (12):

$$T_2(s) = 1 - e^{-2\tau s}.$$

To transform the function $T_2(s)$ from the s-plane to the z-plane, we change the variable s:

$$s = \frac{lnz}{T}.$$

After replacement, the function $T_2(s)$ will take the form:

$$1 - e^{-2\tau s} \to 1 - e^{-2\tau \frac{lnz}{T}} = 1 - z^{-\frac{2\tau}{T}}.$$

Let's denote: $m = 2\tau/T$.
Then:

$$H_2(z) = 1 - z^{-m}. \tag{17}$$

Because the variable z^{-1} is a unit delay operator, m can only take integer values. In other words, the operator z^{-m} corresponds to a signal delay by m clock cycles equal in time to mT quantization steps. Function (17) is the TF of the comb filter [1].

Figure 2(b) it can be seen that the TF $T_2(s)$ forms an infinite set of zeros, scaled along the frequency axis by the coefficient τ. Unlike the analogue frequency scale, the digital one has the property of cyclicity with a period of 2π. Therefore, there is a certain number of zeros per period. It should be borne in mind that the operating range of normalized digital frequencies occupies the interval from 0 to π in the real frequency range. The scaling of the intervals between zeros in (17) is performed by choosing the order of the comb filter m. The number of intervals between zeros in the real digital frequency domain is $m/2$ (if m is even number). In the limit, the number of zeros superimposed over the cycles is infinite, as in the s-plane for $T_2(s)$ as $\omega \to \infty$. As a rule, the number of zeros of $H_2(z)$ should significantly exceed the number of poles of $H_{1l}(z)$. The comb filter has a FR and a PR that are absolutely identical in form to the modulus and the argument of the expression $(1 - e^{-2\tau s})$.

The poles of $H_{1l}(z)$ must exactly match the zeros of $H_2(z)$, i.e., the frequencies x_{kl} in $H_{1l}(z)$ must correspond to the frequencies of the zeros of $H_2(z)$. Consequently, it is very important to express as accurately as possible the coefficients b_{1kl} when implementing a multiband digital filter, which depend on the value of the frequencies x_{kl}. Misalignment of zeros and poles will lead to unwanted spikes in the FR in the frequency domain of the singular points x_{kl}.
The transformed TF of the multiband digital filter will be:

$$H_l(z) = H_{1l}(z)H_2(z) = (1 - z^{-1})^2 \times \\ \times \sum_{kl=1}^{nl} \Big(\frac{A^*_{kl}}{1 + b_{1kl}z^{-1} + z^{-2}}\Big)(1 - z^{-m}), \tag{18}$$

here $b_{1kl} = -2cosx_{kl}$.

Obviously, the TF (18) corresponds to the TF of the FSF [1]. The difference lies in the factor $(1-z^{-1})^2$ and in the normalizing factor $1/m$.

4. MODIFICATION OF THE TRANSFER FUNCTION OF A MULTIBAND DIGITAL FILTER

For the considered TF (18), the approximation problem is reduced to finding the optimal (according to the selected criterion) values of the vector of weight coefficients $\vec{A^*_{kl}}$ minimum dimension (hence the minimum dimension of the polynomial – kl) with the minimum order of the comb filter - m and meeting the specified requirements for passband ripple and guaranteed attenuation in the stopband.

Multiple calculations confirm that in order to successfully solve the approximation problem by the optimization method, it is necessary to have a good initial solution, which is close to the optimal one according to a certain proximity criterion. Only in this case it is possible to achieve a sufficiently fast convergence of the optimization process. Otherwise, the process diverges and an optimal solution cannot be obtained.

The weighting coefficients A^*_{kl} can be easily determined if the interpolation method is used to solve the approximation problem at the first stage. The interpolation means the assignment of discrete points through which the approximating function must pass, at the desired values of the weighting coefficients A^*_{kl}. The

values of the approximating function at singular points and the values of the weighting coefficients have an unambiguous functional dependence. The values of the weighting coefficients found on the basis of this dependence are a fairly good initial approximation for further solving the approximation problem by the optimization method. The need to perform optimization arises because the values of the optimal approximating function at the singular points are not known in advance.

Let's find the analytical ratio for calculating the weighting coefficients A^*_{kl}. For this, it is necessary to carry out a number of mathematical transformations. Let us write down the TF (18), transforming the variable using the Euler formula and highlighting the real and imaginary parts. In the process of transforming the TF of the comb filter included in (18), it is convenient to use De Moivre's formula [24]:

$$\begin{aligned} H_l(jx) = &\Big((1 - 2cosx + cos^2x - sin^2x) + 2j(sinx - cosxsinx)\Big)\times \\ &\times \sum_{kl=1}^{nl} \frac{A^*_{kl}}{1 - 2cosx_{kl}cosx + cos(2x) - j(-2cosx_{kl}sinx + sin(2x))}\times \\ &\times (1 - cos(mx) + jsin(mx)). \end{aligned} \tag{19}$$

As $x \to x_{kl}$, the part of the TF (19), determined by the polynomial under the sum sign, forms the poles, the other factor of the TF $(1 - cos\,(mx) + jsin\,(mx))$ forms zeros. The number of poles corresponds to the dimension of the polynomial under the sum sign, and the number of zeros is equal to $(m/2 + 1)$ on the interval $x\epsilon\,[0, \pi]$, for m even. It is expedient to choose the value m even. Using the above relation to calculate the number of zeros, it is convenient to calculate the frequencies of the singular points x_{kl}, i.e. interpolation nodes. To do this, the interval $[0, \pi]$ is divided into $m/2$ equal sub-intervals, the boundaries of which determine the frequencies x_{kl}. Since the frequencies of the zeros and poles in the filter passband must coincide, it is these values x_{kl} that must be substituted into the expression for calculating the coefficients b_{1kl}. The number of interpolation nodes and coefficients A^*_{kl} must match.

Consequently, the problem arises of finding the values of A^*_{kl} for given values of the modulus of the TF $|H_l(jx)|$ at points of uncertainty of the form $(0/0)$, i.e., at frequencies x_{kl}. To disclose uncertainty, we will use the L'Hôpital's rule [22]. Find the module of the TF $|H_l(jx)|$ as $x \to x_{kl}$. Let us write in more detail, highlighting the part that gives uncertainty and reveal this uncertainty:

$$\begin{aligned} &\lim_{x\to x_{kl}} \left| \frac{1 - \cos(mx) + j\sin(mx)}{1 - 2\cos x_{kl}\cos x + \cos(2x) - j(-2\cos x_{kl}\sin x + \sin(2x))} \times \right. \\ &\left. \times A^*_{kl}((1 - 2\cos x + \cos(2x)) + j(2\sin x - \sin(2x))) \right| \end{aligned}$$

Denote:

$$\begin{aligned} &\lim_{x\to x_{kl}} |\alpha^*| \times |\beta| = \lim_{x\to x_{kl}} \left| \frac{1 - \cos(mx) + j\sin(mx)}{1 - 2\cos x_{kl}\cos x + \cos 2x - j(-2\cos x_{kl}\sin x + \sin 2x)} \right| \times |\beta|, \\ &G_1 = 1 - \cos(mx), \quad G_2 = \sin(mx), \\ &D_1 = 1 - 2\cos x_{kl}\cos x + \cos 2x, \quad D_2 = -2\cos x_{kl}\sin x + \sin 2x, \\ &\beta = A^*_{kl}((1 - 2\cos x + \cos^2 x - \sin^2 x) + 2j(\sin x - \cos x\sin x)). \end{aligned} \tag{20}$$

We write a^* in the form:

$$\alpha^* = \frac{G_1 + jG_2}{D_1 - jD_2} = \frac{G_1D_1 - G_2D_2}{D_1^2 + D_2^2} + j\frac{G_1D_2 + G_2D_1}{D_1^2 + D_2^2}.$$

Taking the first derivative of a^*, the uncertainty cannot be revealed. It is necessary to take the second derivative of a^*:

$$\begin{aligned} a^{*''} = &\frac{(G_1''D_1 + G_1'D_1') + (G_1'D_1' + G_1'D_1'') - (G_2''D_2 + G_2'D_2') + (G_2'D_2' + G_2'D_2'')}{(2(D_1')^2 + 2D_1D_1'') + (2(D_2')^2 + 2D_2D_2'')} + \\ &+ j\frac{(G_1''D_2 + G_1'D_2') + (G_1'D_2' + G_1'D_2'') + (G_2''D_1 + G_2'D_1') + (G_2'D_1' + G_2D_1'')}{(2(D_1')^2 + 2D_1D_1'') + (2(D_2')^2 + 2D_2D_2'')}. \end{aligned} \tag{21}$$

Taking into account that some terms of equality (21) are equal to 0 as $x \to x_{kl}$, we can write:

$$\lim_{x \to x_{kl}} a^{*''} = \frac{G_1^{'} D_1^{'} - G_2^{'} D_2^{'}}{(D_1^{'})^2 + (D_2^{'})^2} + j \frac{G_1^{'} D_2^{'} + G_2^{'} D_1^{'}}{(D_1^{'})^2 + (D_2^{'})^2} = \alpha_1 + j\alpha_2. \tag{22}$$

$$\begin{aligned} G_1' &= -m\sin(mx); & G_2' &= m\cos(mx); \\ D_1' &= -2\sin x_{kl}\cos x_{kl}; & D_2' &= -2\sin^2 x_{kl}. \end{aligned} \tag{23}$$

Since $x \in [0, \pi]$, then:

$$G_1^{'} = 0; G_2^{'} = m. \tag{24}$$

Taking into account (23), (24), we write:

$$\begin{aligned} \alpha_1 &= \frac{-G_2' D_2'}{(D_1')^2 + (D_2')^2} = \frac{-m(-2\sin^2 x_{kl})}{(-2\sin x_{kl}\cos x_{kl})^2 + (-2\sin^2 x_{kl})^2} = \frac{m}{2}; \\ \alpha_2 &= \frac{G_2' D_1'}{(D_1')^2 + (D_2')^2} = \frac{m(-2\sin x_{kl}\cos x_{kl})}{(-2\sin x_{kl}\cos x_{kl})^2 + (-2\sin^2 x_{kl})^2} = -\frac{m}{2}\cot x_{kl}. \end{aligned} \tag{25}$$

The modulus of expression (22), taking into account (25), will be equal to:

$$\lim_{x \to x_{kl}} |\alpha^{*''}| = \sqrt{\alpha_1^2 + \alpha_2^2} = \frac{m}{2 sin x_{kl}}.$$

Referring to (20), as $x \to x_{kl}$ we can write:

$$\beta|_{x \to x_{kl}} = A_{kl}^{*}(1 - cosx_{kl} + cos^2 x_{kl} - sin^2 x_{kl}) + 2j(sinx_{kl} - cosx_{kl} sinx_{kl}). \tag{26}$$

Let us make identical transformations in (26) in order to simplify and bring to a convenient form. Then:

$$\beta|_{x \to x_{kl}} = 2A_{kl}^{*}(1 - cosx_{kl})(cosx_{kl} - jsinx_{kl}). \tag{27}$$

The modulus of expression (27) will be:

$$|\beta|_{x \to x_{kl}}| = |2A_{kl}^{*}(1 - cosx_{kl})|,$$

because: $|cosx_{kl} - jsinx_{kl}| = 1$.
Thus:

$$|H_l(jx)|_{x \to x_{kl}}| = \lim_{x \to x_{kl}} |\alpha^{*''}| \times |\beta| = |A_{kl}^{*} m tan \frac{x_{kl}}{2}|. \tag{28}$$

Turning to a logarithmic scale, the analytical ratio for calculating the weighting coefficients can be written:

$$A_{kl}^{*} = (-1)^{q+1} \frac{10^{-\frac{a_{kl}}{20}}}{m tan \frac{x_{kl}}{2}}, \tag{29}$$

here $q = 0, 1, 2, \ldots$;
a_{kl} (dB): the specified value of the attenuation of the approximating function at the interpolation node.

Since the phases in the sequence of elementary filters at resonance differ by π, the transmission coefficients of all elementary filters with odd (even) numbers should be multiplied by (-1). Therefore, the composition (29) includes the factor $(-1)^{q+1}$.

Referring to (29), we can see that, in the general case, the frequency dependence of the coefficients A_{kl}^{*} can be represented as the graph of the function $\frac{1}{tan(x/2)}$, shown in Figure 3.

Expected result: the bilinear z-transform does not preserve the identity of the FR of the analog and digital filters, however, the shape of their frequency characteristics remains the same [1]. This is due to the nonlinear relationship between digital and analog frequencies. Therefore, the weighting coefficients A_{kl}^{*}, which

are frequency dependent, take on values according to the function of the half tangent argument. Therefore, there is an asymmetry in the transfer coefficients of the TF (18) at the interpolation nodes.

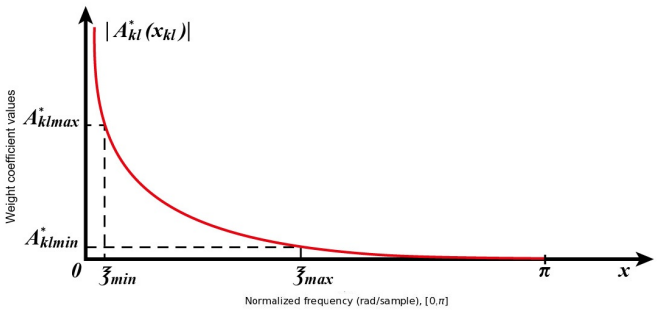

Figure 3. Graph of the function $\frac{1}{tan(x/2)}$

The analysis of the above results suggests that it is advisable to introduce a weight function into the TF (18), which will make it possible to achieve a linear dependence of the coefficients A^*_{kl} on frequency.

After analyzing (28), we can come to the conclusion that it is necessary to introduce a scaling factor $1/m$ into the composition of the TF (18) and a factor whose module corresponds to the function $cot(x/2)$. The weighting function $cot(x/2)$ is implemented using the link:

$$\frac{1+z^{-1}}{1-z^{-1}}. \tag{30}$$

The modulus of the weighting function (30) is equal to:

$$\left|\frac{1+e^{-jx}}{1-e^{-jx}}\right| = \frac{|2e^{-(\frac{jx}{2})}cos(x/2)|}{|j2e^{-(\frac{jx}{2})}sin(x/2)|} = \frac{|cos(x/2)|}{|sin(x/2)|} = |cot(x/2)|.$$

Therefore, after substituting the weighting function (30) into the TF (18), the modified (alternative) TF will take the form [2], [25]:

$$H_l(z) = (1-z^{-m})(\frac{1}{m})(1-z^{-2})\sum_{kl=1}^{nl}\frac{(-1)^k A_{kl}}{1-2cos(\frac{2\pi k}{m})z^{-1}+z^{-2}}. \tag{31}$$

For the modified TF (31), the calculated ratio by which the values of the weighting coefficients A_{kl} are calculated will take the form:

$$\begin{aligned} A_{kl} &= (-1)^{q+1}10^{-\frac{a_{kl}}{20}}, \\ A_{kl} &= (-1)^{q+1}|H_l(jx_k)|. \end{aligned} \tag{32}$$

It is obvious that the weighting coefficients A_{kl} (32) of the TF (31) is frequency independent.

For a visual illustration of the frequency independence of the weighting coefficients A_{kl} (32) of the modified FSF TF with real coefficients (31) below are graphs of magnitude response (MR) of its components. In Figure 4 shows the MR of twelve resonators:

$$H1(z) = \sum_{k=1}^{13}\frac{A_k \times (-1)^k}{1+b_{1k}z^{-1}+b_2 z^{-2}}, \tag{33}$$

here $m = 28$;
$k = m/2$;
$A_k = 1$;
$d = 14$ (bit width);
$b_2 = 1 - 2^{-d}$;

$r = \sqrt{b_2}$ (polar distance);
$b_{1k} = -2rcos(\frac{2\pi k}{m})$;
$x_k = \frac{2\pi k}{m}$.

All weighting coefficients (33) $A_k = 1$. In order to better visualize the extreme values of the MR of digital resonators on the graphs, the poles (33) are shifted to the middle of the unit circle of the z-plane $\left(r = \sqrt{1 - 2^{-14}}\right)$.

In Figure 4 clearly shows that the extremes of MR (33) have a nonlinear dependence on frequency. In Figure 5 shows the MR of the comb filter of the 2nd order, which is part of the TF (31):

$$H2(z) = (1 - z^{-2}). \tag{34}$$

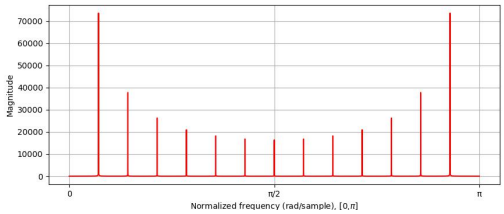

Figure 4. Magnitude response of the transfer function (33)

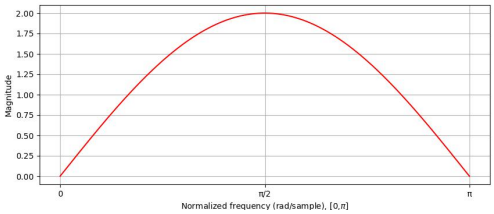

Figure 5. Magnitude response of the transfer function (34)

In Figure 6 shows the MR, which is determined by the modulus of the function:

$$H3(z) = (1 - z^{-2}) \sum_{k=1}^{13} \frac{A_k \times (-1)^k}{1 + b_{1k} z^{-1} + b_2 z^{-2}}. \tag{35}$$

In Figure 6 clearly shows that the nonlinearity of extrema, which is observed in Figure 4 compensated.

Let us consider a general example. The transfer functions of bandpass filters based on TF (31) (with m=28 and all $A_k = 1$) will have the following form:

$$H4(z) = (1 - z^{-28}) \frac{1}{28} (1 - z^{-2}) \sum_{k=5}^{8} \frac{1 \times (-1)^k}{1 - 2cos(\frac{2\pi k}{28}) z^{-1} + z^{-2}}. \tag{36}$$

$$H5(z) = (1 - z^{-28}) \frac{1}{28} (1 - z^{-2}) \sum_{k=7}^{10} \frac{1 \times (-1)^k}{1 - 2cos(\frac{2\pi k}{28}) z^{-1} + z^{-2}}. \tag{37}$$

The MR of the TF (36) and (37) at the interpolation nodes takes on a value equal to that of the corresponding k-th weight coefficient $A_k = 1$ (Figure 7). Curve 1 – The magnitude response of TF (36). Curve 2 – The magnitude response of TF (37).

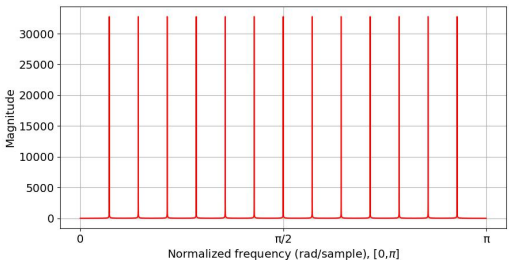

Figure 6. Magnitude response of the transfer function (35)

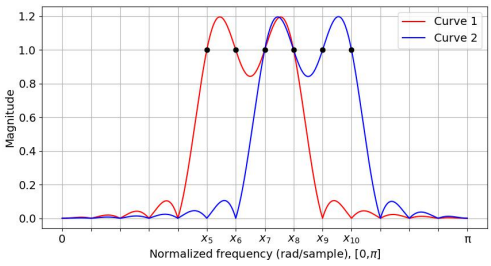

Figure 7. Magnitude responses of the transfer functions (36), (37)

In the above example (Figure 7), we have clearly demonstrated that the vector of weight coefficients $\overrightarrow{A_{kl}}$ (32) of the modified TF (31) is independent of frequency in the entire operating frequency range of the filter. The MR of TF (31) at an interpolation node will always equal the value of the corresponding weight coefficient. This property provides useful opportunities for the approximation of FSF and FSF banks.

It is advisable for the weighting coefficients of the resonators in the TF of the FSF (31), which form the passband of the filter, to be equal to one. However, in this case, the passband ripple may be unsatisfactory. When the number of resonators exceeds four, characteristic peaks appear at the edges of the passband in the MR (Figure 8, Curves 1 and 4). In such cases, one can optimize the weighting coefficients (for example, one can perform optimization using the Chebyshev criterion) to reduce the ripple in the passband. However, after optimization, the coefficients will no longer be equal to one.

There is an alternative approach. The weighting coefficients in the passband can be kept equal to one, and only those located at the edges of the passband can be modified. We refer to them as Gibbs coefficients - G. As a result, the passband ripple will be significantly reduced, while the weighting coefficients within the passband remain equal to one. The Gibbs coefficients will be less than one (Figure 8, Curves 2 and 3).

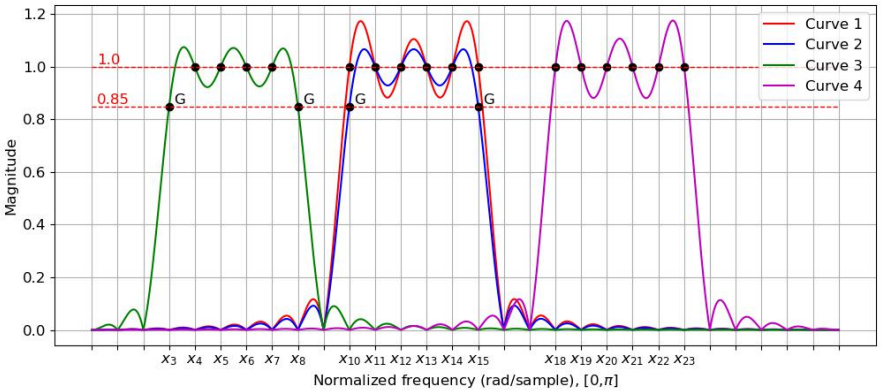

Figure 8. Magnitude responses of the transfer functions (38)-(41)

Curve 1 – The magnitude response of TF (38):

$$H6(z) = (1 - z^{-58})\frac{1}{58}(1 - z^{-2}) \sum_{k=10}^{15} \frac{A_k \times (-1)^k}{1 + 2cos(\frac{2\pi k}{58})z^{-1} + z^{-2}}, \tag{38}$$

here m=58;
A_{10}=1; A_{11}=1; A_{12}=1; A_{13}=1; A_{14}=1; A_{15}=1.
Curve 2 – The magnitude response of TF (39):

$$H7(z) = (1 - z^{-58})\frac{1}{58}(1 - z^{-2}) \sum_{k=10}^{15} \frac{A_k \times (-1)^k}{1 + 2cos(\frac{2\pi k}{58})z^{-1} + z^{-2}}, \tag{39}$$

here m=58;
$G = A_{10}$=0.85; A_{11}=1; A_{12}=1; A_{13}=1; A_{14}=1; $G = A_{15}$=0,85;
G - Gibbs coefficient.
Curve 3 – The magnitude response of TF (40):

$$H8(z) = (1 - z^{-58})\frac{1}{58}(1 - z^{-2}) \sum_{k=3}^{8} \frac{A_k \times (-1)^k}{1 + 2cos(\frac{2\pi k}{58})z^{-1} + z^{-2}}, \tag{40}$$

here m=58;
$G = A_3$=0.85; A_4=1; A_5=1; A_6=1; A_7=1; $G = A_8$=0,85;

G - Gibbs coefficient.

Curve 4 – The magnitude response of TF (41):

$$H9(z) = (1 - z^{-58})\frac{1}{58}(1 - z^{-2}) \sum_{k=18}^{23} \frac{A_k \times (-1)^k}{1 + 2cos(\frac{2\pi k}{58})z^{-1} + z^{-2}}, \tag{41}$$

here m=58;

A_{18}=1; A_{19}=1; A_{20}=1; A_{21}=1; A_{22}=1; A_{23}=1.

When designing filters, it is important to consider the effect of quantization of the TF coefficients on the resulting FR. A detailed analysis of the sensitivity of coefficients to quantization of the modified FSF TF with real coefficients (31) is presented in [26].

Attention should be paid to the specific properties of the feedback coefficients of the resonators - $b_{1k} = -2cos(2\pi k/m)$ in the TF (31). These coefficients are the most sensitive. They are calculated as the roots of a second-order equation and determine the center frequencies of the resonators (i.e., the poles of the FR). The greater the separation between a pole and a zero, the more the frequency characteristics become distorted. The feedback coefficients lie within the interval [-2, 2]. The sensitivity of the coefficients b_{1k} to quantization in the operating frequency range is nonlinear. Their sensitivity is highest at frequencies close to 0 and π, and lowest near $\frac{\pi}{2}$, forming a symmetric pattern around $\frac{\pi}{2}$. This nonlinear sensitivity is due to the fact that quantization of coefficient values near -2 and 2 causes larger shifts in the resonator frequency compared to quantization near 0. To visually demonstrate this nonlinear dependence, the graph below shows the functional dependence of the feedback coefficient on frequency: $-2cos\,(x)$ (Figure 9).

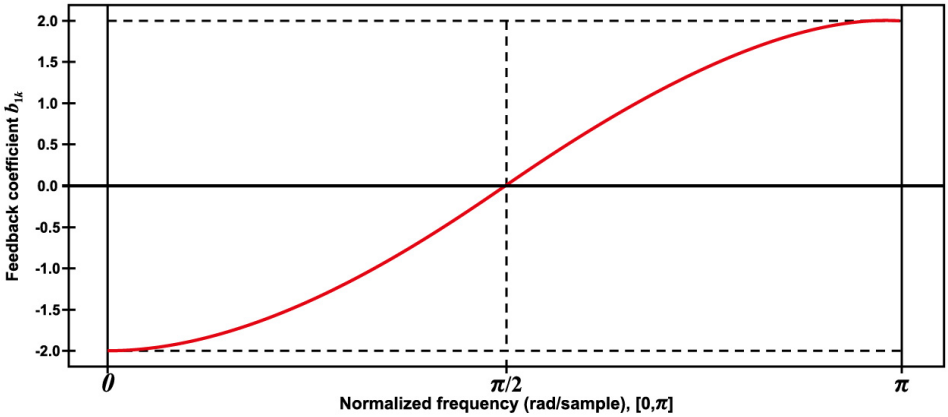

Figure 9. Graph of the frequency dependence of the feedback coefficient b_{1k}

This property of the feedback coefficients leads to an uneven distribution of poles in the z-plane during quantization.

5. IMPROVED RYBKA-LYONS FSF BLOCK DIAGRAM

Figure 10 shows an improved Rybka-Lyons FSF block diagram, based on the modified (alternative) transfer function (31). FSFs are made up of a simple comb filter whose output is applied to a bank of guaranteed-stable resonators. Each resonator has a different resonant frequency.

The IR of any given resonator, driven by the comb filter, is an exact integer number of cycles of a sinusoidal sequence whose frequency is the resonant frequency of the resonator. This tells us the FR of a given resonator is equivalent to the convolution of the FSF filter's input and a tapped-delay line FIR filter whose IR is an exact integer number of cycles of a sinusoidal sequence whose frequency is the resonant frequency of the resonator [2].

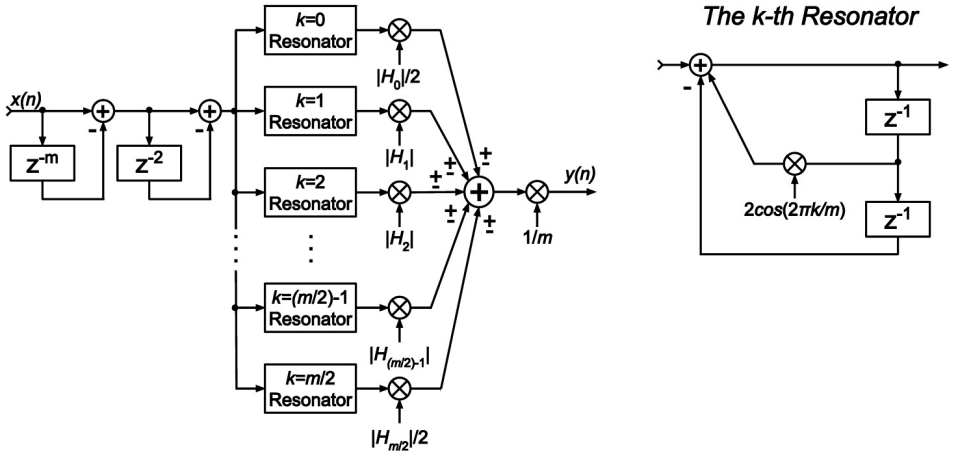

Figure 10. Improved Rybka-Lyons FSF block diagram

As such, an FSF is equivalent to a bank of linear-phase FIR narrowband bandpass filters. The frequency resolution (frequency granularity) available to us in designing an FSF is the inverse of the comb filter's delay length - m, of the comb filter. Thus, the larger is m the finer (higher resolution) frequency control we have over an FSFs FR. Each resonator generates a single subband of an FSFs FR. The sum of multiple consecutive subbands create the desired bandpass of the FSF. The output signal of each resonator is multiplied by a gain coefficient, whose value is between zero and one, which controls the MR of that resonator's frequency subband. The weighting coefficients are frequency independent in the entire working frequency range. The zeros of the comb filter and the poles of the guaranteed stable resonators are located on the unit circle of the z-plane. The radius of their poles and zeros is equal to unity. The poles of a second-order resonator with real coefficients will never lie outside the unit circle in the z-plane.

Quantizing the feedback coefficient of a single-resonator FSF $b_{1k} = -2cos(2\pi k/m)$ will result in a slight displacement of the cavity poles along the unit circle relative to the desired positions on the z-plane unit circle. The amount of unwanted angular displacement of the quantized pole is predictable and inversely proportional to the number of binary bits used to represent the feedback coefficient.

This unfortunate fact is compounded by the non-uniform pole distribution characteristics of our 2nd-order resonator structure, as discussed in the literature [27]-[30]. So, this inexact pole/zero cancellation, due to a quantized feedback coefficient, causes the FSFs IR to no longer be finite in duration as we desire.

The unwanted residual sinusoids' peak amplitudes depend on how many feedback coefficient magnitude bits are used, and a resonator's k value. When an FSFs feedback coefficient is represented with double precision floating point numbers (IEEE Standard 754) the unwanted residual sinusoid's amplitudes will be more than 275 dB below (m=64) that of the initial desired IR sinusoid for all vales of k.

The above information makes think that when an FSF resonators' feedback coefficients are represented by a sign bit and 15 magnitude bits then the FSFs performance will be fairly good. And when the feedback coefficients are represented by a sign bit and 31 magnitude bits, or floating-point numbers, the FSFs performance will be very good.

FSFs are convenient for constructing filter banks. In this case, we consider a filter bank as a system with a single input and l independent outputs. Each output corresponds to its own passband with a specified ripple and stopbands with guaranteed attenuation. All outputs have a linear PR.

The improved Rybka-Lyons FSF bank block diagram consists of a simple comb filter (a shift register), whose output signal is fed to a set of guaranteed stable resonators, distributed among the l-outputs (Figure 11). The shared use of the comb filter by all l-outputs significantly increases the efficiency of the filter bank. All components of the FSF bank are standard elements and are well studied for both hardware and software implementation.

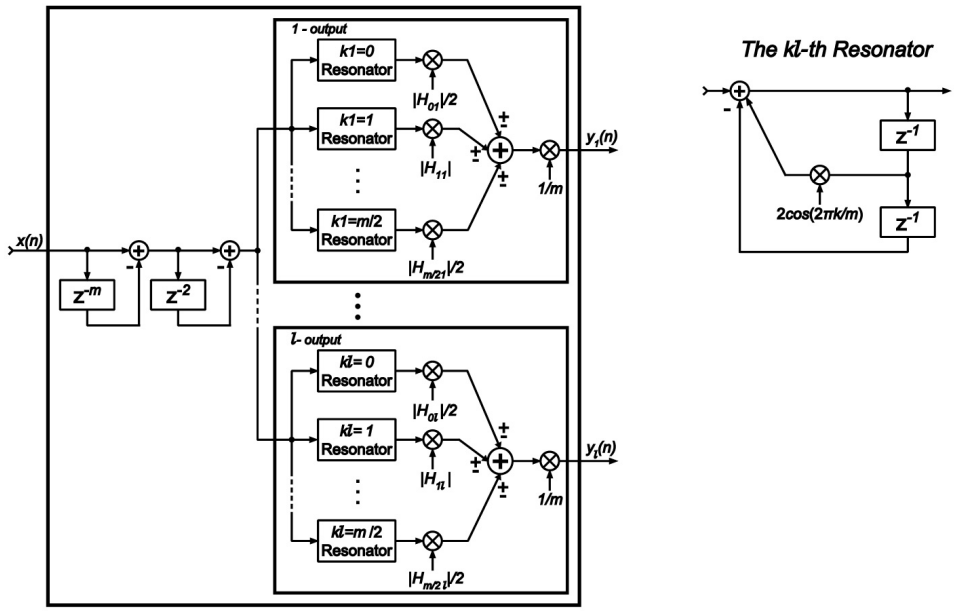

Figure 11. Improved Rybka-Lyons FSF bank block diagram

6. EXAMPLES OF PREVIOUSLY CALCULATED BANDPASS FSFS AND FSF BANK

Solving the approximation problem in the design of digital filters is one of the most difficult problems in digital signal processing. The difficulty lies in the fact that this problem is a nonlinear programming problem and it does not have a canonical solution. For FSFs with two or more transition weights, the problem of their approximation is a nonlinear programming problem.

The approximation problem can be successfully solved if, to ensure rapid convergence of the optimization process, the initial approximation is chosen from outside the region of nonlinear behavior. Depending on the selected initial approximation, the resulting solution, with respect to the accuracy of reproducing the given FR, may be either globally or locally optimal. To determine which type of optimum has been reached, a clearly defined analytical criterion is required (as in the case of the well-defined Chebyshev criterion). An unsubstantiated statement such as "a minimum or maximum value is reached" is insufficient. Any filter design method that does not establish explicit criteria for evaluating optimization results is questionable in terms of the optimality of the obtained solution.

In this case, when solving the problem of approximation of the TF (31), it is necessary to solve the so-called dual problem [31]. Namely, to achieve the minimum minimorum (the smallest value in the data series) or the given value of unevenness in the passband - $\Delta a(x, \vec{A_k})$ while simultaneously achieving the maximum maximorum (the largest value in the data series) of the guaranteed attenuation in the filter stopband - $a_g(x, \vec{A_k})$ and meeting the requirements for the filter cutoff frequencies.

The formalized filter approximation problem is written using a system of inequalities:

$$\begin{cases} max\Delta a(x, \vec{A_k}) \leq \Delta a_{minmin} \; in \; the \; passband; \\ min a_g(x, \vec{A_k}) \geq a_{g \; maxmax} \; in \; the \; stopband. \end{cases} \tag{42}$$

The system of inequalities (42) is a nonlinear programming problem, for the solution of which it is advisable to use the method of linearization of functions in combination with linear programming. It is this method that provides a higher convergence rate of the optimization process for this class of problems compared to other methods of mathematical programming.

A separate article will be devoted to the technology of solving the FSF approximation problem based on the modified TF (31). It is important to note that the study of methods for approximating the analog prototype (Figure 1) [15]–[20] allowed us to successfully apply the knowledge obtained to solve the FSF approximation

problem. Below are the results of the FSF calculations based on the TF:

$$H(z) = (1 - z^{-182})\frac{1}{182}(1 - z^{-2}) \sum_{k=40}^{51} \frac{(-1)^k A_{kl}}{1 - 2cos(\frac{2\pi k}{182})z^{-1} + z^{-2}},$$

where: m = 182: comb filter order;
$k \in \{0; 182/2\}$: interpolation node numbers;
K = 4: the number of weighting coefficients in the passband whose values are equal to unity A_k=1;
T = 3: number of transitional weighting coefficients;
G: the Gibbs coefficient.

From the beginning, an absolutely symmetrical variant is calculated with respect to the main axis of symmetry of the working range of normalized digital frequencies - $\pi/2$. Calculation of an absolutely symmetrical solution reduces the effort and time spent on solving the approximation problem for each individual output of the filter bank. The obtained absolutely symmetrical solution can be used to form the frequency characteristics of all outputs of the filter bank. This will be shown below.

The values of the weighting coefficients of the bandpass FSF are given in Table 1. The weighting coefficients in the passband A_k are chosen to be equal to unity in order to simplify the multiplication operations when implementing the filter. The value of the normalizing coefficient ns=1.00121. Attenuation characteristic of this filter is shown in Figure 12.

Table 1. The group of weighting coefficients of the bandpass FSF (m = 182, G, K = 4, T = 3)

Number	Values
$T_3 = A_{40}$	0.0085126003129317
$T_2 = A_{41}$	0.12125309882399
$T_1 = A_{42}$	0.484835416765368
$G = A_{43}$	0.881197891235345
A_{44}	1
A_{45}	1
A_{46}	1
A_{47}	1
$G = A_{48}$	0.881197891235345
$T_1 = A_{49}$	0.484835416765368
$T_2 = A_{50}$	0.12125309882399
$T_3 = A_{51}$	0.0085126003129317

Parameters of attenuation characteristic:
$\Delta a = 0.0138\ dB$ (passband ripple);
$a_g = -105.0\ dB$ (stopband attenuation). If you increase the permissible ripple value in the filter's passband, this will allow you to widen the passband in frequency. This, in turn, makes it possible to smoothly adjust the filter's cutoff frequencies within a single interval between the zeros of the comb filter. Additionally, increasing the passband ripple enables a higher guaranteed attenuation value in the stopband.

To obtain the weighting coefficients of the FSF bank, we apply the property of identity (uniformity) of the weighting coefficients of the absolutely symmetric solution (Table 1). The obtained weighting coefficients for the FSF bank with thirteen outputs are presented in Table 2.
The corresponding modified TF FSF bank based on Table 2 would be as follows:

$$H_{1-13}(z) = (1 - z^{-182}) \times \frac{1}{182} \times \frac{1}{n_s} \times (1 - z^{-2}) \times \begin{cases} \sum_{k1=4}^{15} \frac{A_{k1}(x_k)\times(-1)^{k1}}{1+b_{1k1}z^{-1}+z^{-2}}; \\ \sum_{k2=10}^{21} \frac{A_{k2}(x_k)\times(-1)^{k2}}{1+b_{1k2}z^{-1}+z^{-2}}; \\ \vdots \\ \sum_{k13=76}^{87} \frac{A_{k13}\times(-1)^{k13}}{1+b_{1k13}z^{-1}+z^{-2}}, \end{cases}$$

where:

$$b_{1k} = -2cos(\frac{2\pi k}{182}).$$

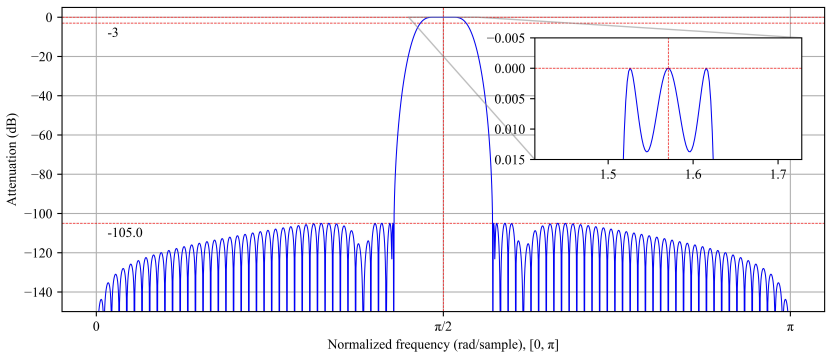

Figure 12. Attenuation characteristic of a bandpass FSF (m = 182, G, K = 4, T = 3)

Table 2. Weighting coefficients $A_{kl}(x_k)$ of bandpass FSFs bank on its individual outputs ($l = 1 - 13, m = 182, G, K = 4, T = 3$)

l=1	l=2	l=3	l=4	l=5	l=6	l=7	l=8	l=9	l=10	l=11	l=12	l=13	Values
$A_{4,1}$	$A_{10,2}$	$A_{16,3}$	$A_{22,4}$	$A_{28,5}$	$A_{34,6}$	$A_{40,7}$	$A_{46,8}$	$A_{52,9}$	$A_{58,10}$	$A_{64,11}$	$A_{70,12}$	$A_{76,13}$	$T_3 = 0.0085126003129317$
$A_{5,1}$	$A_{11,2}$	$A_{17,3}$	$A_{23,4}$	$A_{29,5}$	$A_{35,6}$	$A_{41,7}$	$A_{47,8}$	$A_{53,9}$	$A_{59,10}$	$A_{65,11}$	$A_{71,12}$	$A_{77,13}$	$T_2 = 0.12125309882399$
$A_{6,1}$	$A_{12,2}$	$A_{18,3}$	$A_{24,4}$	$A_{30,5}$	$A_{36,6}$	$A_{42,7}$	$A_{48,8}$	$A_{54,9}$	$A_{60,10}$	$A_{66,11}$	$A_{72,12}$	$A_{78,13}$	$T_1 = 0.484835416765368$
$A_{7,1}$	$A_{13,2}$	$A_{19,3}$	$A_{25,4}$	$A_{31,5}$	$A_{37,6}$	$A_{43,7}$	$A_{49,8}$	$A_{55,9}$	$A_{61,10}$	$A_{67,11}$	$A_{73,12}$	$A_{79,13}$	$G = 0.881197891235345$
$A_{8,1}$	$A_{14,2}$	$A_{20,3}$	$A_{26,4}$	$A_{32,5}$	$A_{38,6}$	$A_{44,7}$	$A_{50,8}$	$A_{56,9}$	$A_{62,10}$	$A_{68,11}$	$A_{74,12}$	$A_{80,13}$	$= 1$
$A_{9,1}$	$A_{15,2}$	$A_{21,3}$	$A_{27,4}$	$A_{33,5}$	$A_{39,6}$	$A_{45,7}$	$A_{51,8}$	$A_{57,9}$	$A_{63,10}$	$A_{69,11}$	$A_{75,12}$	$A_{81,13}$	$= 1$
$A_{10,1}$	$A_{16,2}$	$A_{22,3}$	$A_{28,4}$	$A_{34,5}$	$A_{40,6}$	$A_{46,7}$	$A_{52,8}$	$A_{58,9}$	$A_{64,10}$	$A_{70,11}$	$A_{76,12}$	$A_{82,13}$	$= 1$
$A_{11,1}$	$A_{17,2}$	$A_{23,3}$	$A_{29,4}$	$A_{35,5}$	$A_{41,6}$	$A_{47,7}$	$A_{53,8}$	$A_{59,9}$	$A_{65,10}$	$A_{71,11}$	$A_{77,12}$	$A_{83,13}$	$= 1$
$A_{12,1}$	$A_{18,2}$	$A_{24,3}$	$A_{30,4}$	$A_{36,5}$	$A_{42,6}$	$A_{48,7}$	$A_{54,8}$	$A_{60,9}$	$A_{66,10}$	$A_{72,11}$	$A_{78,12}$	$A_{84,13}$	$G = 0.881197891235345$
$A_{13,1}$	$A_{19,2}$	$A_{25,3}$	$A_{31,4}$	$A_{37,5}$	$A_{43,6}$	$A_{49,7}$	$A_{55,8}$	$A_{61,9}$	$A_{67,10}$	$A_{73,11}$	$A_{79,12}$	$A_{85,13}$	$T_1 = 0.484835416765368$
$A_{14,1}$	$A_{20,2}$	$A_{26,3}$	$A_{32,4}$	$A_{38,5}$	$A_{44,6}$	$A_{50,7}$	$A_{56,8}$	$A_{62,9}$	$A_{68,10}$	$A_{74,11}$	$A_{80,12}$	$A_{86,13}$	$T_2 = 0.12125309882399$
$A_{15,1}$	$A_{21,2}$	$A_{27,3}$	$A_{33,4}$	$A_{39,5}$	$A_{45,6}$	$A_{51,7}$	$A_{57,8}$	$A_{63,9}$	$A_{69,10}$	$A_{75,11}$	$A_{81,12}$	$A_{87,13}$	$T_3 = 0.0085126003129317$

The attenuation characteristics of the FSF bank are shown in Figure 13. This figure shows that the attenuation characteristics in the stopbands slightly decrease near the left and right boundaries of the operating frequency range of the FSF bank due to asymmetry.

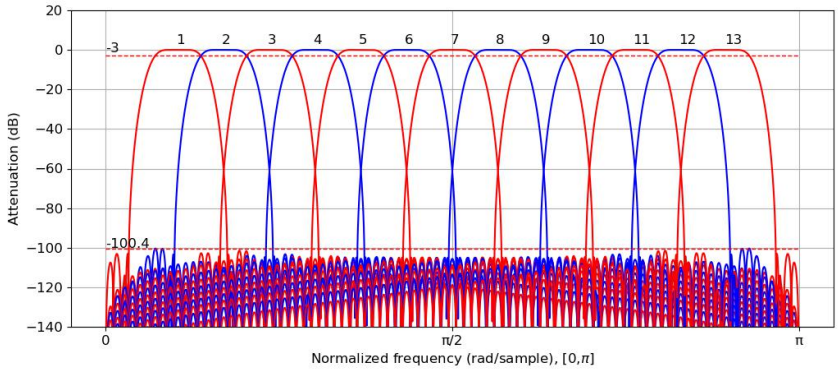

Figure 13. FSF bank attenuation characteristics

The attenuation parameters for the bandpass FSFs located near the boundaries of the operating frequency range have the following values:

$\Delta a = 0.0139\ dB$ (passband ripple);

$a_g = -100.01\ dB$ (stopband attenuation).

The use of the identity property of the weighting coefficients across the outputs of the filter bank increases its implementation efficiency through coefficient unification. However, it is also possible to perform separate calculations for each output of the bank in order to achieve the specified attenuation characteristics. In this case, the coefficients at the different outputs of the FSFs bank will not be identical.

7. COMPARISON OF CLASSICAL AND ALTERNATIVE METHODS FOR OBTAINING TRANSFER FUNCTIONS OF FREQUENCY SAMPLING FILTERS AND THEIR FREQUENCY CHARACTERISTICS

The classical frequency-sampling method is an independent procedure for the synthesis of digital FIR-filters, which is based on a mathematically strictly defined sequence of operations and does not rely on an analog prototype. In this method, the TF of the filter is defined in the frequency domain in the form of a discrete set of values at equally spaced frequencies, after which the IR is obtained by the inverse discrete Fourier transform (IDFT). Since the IR and its discrete Fourier transform (DFT) are mutually uniquely determined (within the period N), the weight coefficients of the FIR-filter can be expressed directly through the DFT-coefficients. As a result, the classical basic TF of a recursive FSF in complex form is obtained [2], [3], [6], [7], [13], [31]–[40]:

$$H(z) = \frac{1 - z^{-N}}{N} \sum_{k=0}^{N-1} \frac{H(k)}{1 - z^{-1} e^{-i(2\pi/N)k}}. \tag{43}$$

The TF (43) formally has complex coefficients; therefore, its implementation requires a quadrature structure in which the real and imaginary parts are processed in parallel. The first-order complex sections of the TF (43) can be grouped into complex-conjugate pairs and implemented as second-order sections with real coefficients [32]. According to publications on the topic of FSF, the FSF TF with real coefficients are those that are most widely used in practice.

It should be emphasized that, in the justification of the frequency-sampling method, the discussion concerns the values of the MR at discrete, equally spaced frequencies, which are defined through the corresponding DFT-coefficients of the TF of the digital filter. Requirements for the PR are not imposed at this stage of the justification of TF (43).

In [13], during the discussion of the design technique–frequency sampling, a fundamental condition is formulated under which the PR of the recursive FSF TF is linear (subsection 3.17, 3.18, 3.21, and 3.22). Briefly, this condition requires that the frequency samples satisfy the complex-conjugate symmetry; therefore, the IR is real and symmetric (or antisymmetric). Accordingly, the zeros and poles of the FSF TF are mirror-symmetrically located with respect to the real axis of the z-plane (i.e., they form complex conjugate pairs). All coefficients of the equivalent realization are real.

A concise analysis of the main classical types of FSF TF is presented below. Beforehand the following conditions for all TFs to be analyzed are defined:

- The order of the comb filter is N = 26;
- All weighting coefficients of the TF are set to unity;
- In the transition band, weighting coefficients are not applied.

Let us begin with the FSF TF in the complex form (43). The low-pass FSF TF with an odd number of resonators (seven resonators) can be expressed in the complex form as:

$$HC1_{odd}(z) = (1 - z^{-26}) \frac{1}{26} \sum_{k=0}^{6} \frac{(-1)^k \times 1}{1 - e^{i(\frac{2\pi k}{26})} z^{-1}}, \tag{44}$$

where x denotes the normalized digital frequency, $x \in [0,\ \pi]$.

Figure 14 presents the frequency characteristics of TF (44), namely, the magnitude response, phase response, and group delay. The impulse response and the zero diagram of TF (44) are also shown. This order of presenting TF characteristics will be followed throughout the text.

A concise analysis of the characteristics shown in Figure 14, corresponding to TF (44), is as follows:

a. The MR corresponds to the specified values of the frequency samples at the interpolation nodes.
b. The PR is generally nonlinear; however, a nearly linear-phase region is observed within the passband.

c. The group delay (GD) is nonconstant.
d. The IR has a complex form and is not symmetric.
e. The pole–zero plot in the z-plane shows that Hermitian (complex-conjugate) symmetry is absent, which indicates the complex nature of TF (44); the radial symmetry of the zeros is violated.

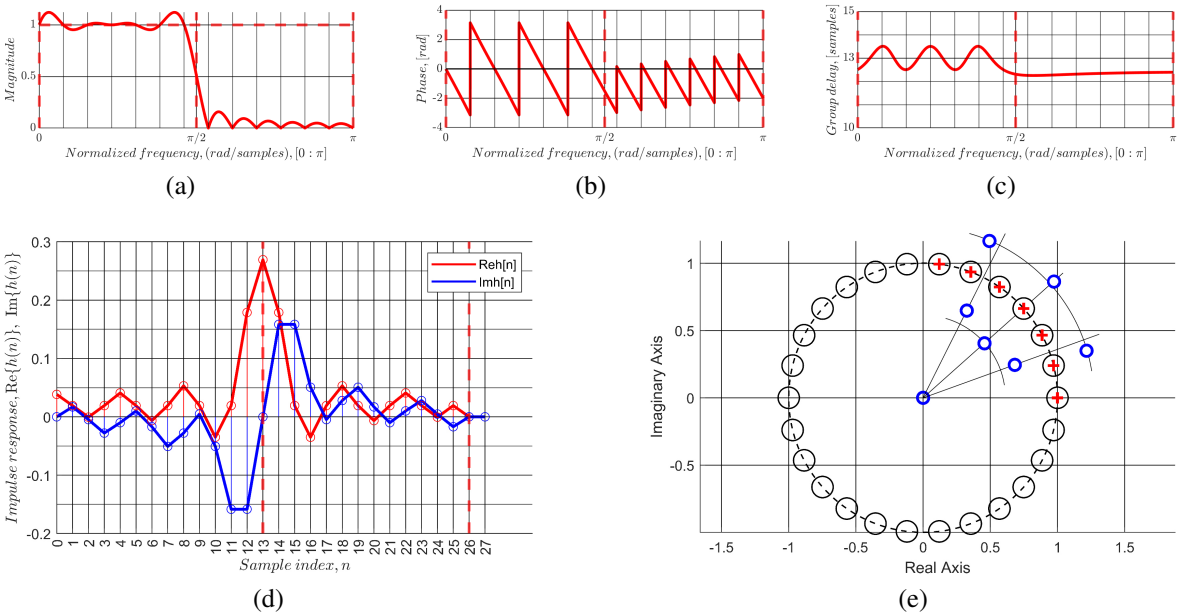

Figure 14. Characteristics of the transfer function (44) $HC1_{odd}(z)$: (a) magnitude response; (b) phase response; (c) group delay; (d) impulse response; and (e) pole-zero plot in the z-plane

Let us write the *low-pass* FSF TF in the *complex form* with an *even* number of resonators (six resonators):

$$HC1_{even}(z) = (1 - z^{-26})\frac{1}{26}\sum_{k=0}^{5}\frac{(-1)^k \times 1}{1 - e^{i(\frac{2\pi k}{26})}z^{-1}}. \tag{45}$$

Figure 15 shows the characteristics of TF (45). A concise analysis of the characteristics shown in Figure 15, corresponding to TF (45), is as follows:

a. The MR corresponds to the specified values of the frequency samples at the interpolation nodes.
b. The PR is quasi-linear due to the symmetry of the interpolation nodes and the paired set of resonators.
c. The GD is constant.
d. The IR is real and symmetric.
e. The pole–zero plot in the z-plane shows that Hermitian symmetry is absent, which indicates the complex nature of TF (45); the zeros are radially symmetric.

Let us write the *band-pass* FSF TF in the *complex form* with an *odd* number of resonators (five resonators):

$$HC1_{odd}(z) = (1 - z^{-26})\frac{1}{26}\sum_{k=5}^{9}\frac{(-1)^k \times 1}{1 - e^{i(\frac{2\pi k}{26})}z^{-1}}. \tag{46}$$

Figure 16 shows the characteristics of TF (46). A concise analysis of the characteristics shown in Figure 16, corresponding to TF (46), is as follows:

a. The MR corresponds to the specified values of the frequency samples at the interpolation nodes.
b. The PR is generally nonlinear; however, a nearly linear-phase region is observed within the passband.
c. The GD is nonconstant.
d. The IR has a complex form and is not symmetric.

e. The pole–zero plot in the z-plane shows that Hermitian symmetry is absent, which indicates the complex nature of TF (46); the radial symmetry of the zeros is violated.

Let us write the *band-pass* FSF TF in the *complex form* with an *even* number of resonators (four resonators):

$$HC2_{even}(z) = (1 - z^{-26})\frac{1}{26}\sum_{k=5}^{8}\frac{(-1)^k \times 1}{1 - e^{i(\frac{2\pi k}{26})}z^{-1}}. \tag{47}$$

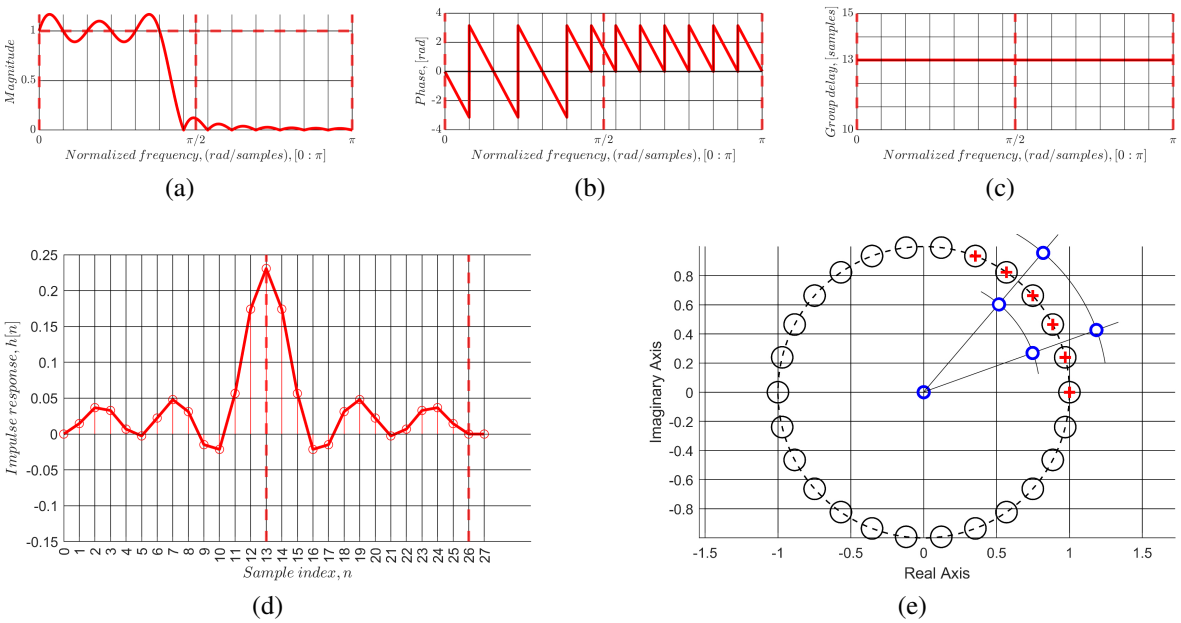

Figure 15. Characteristics of the transfer function (45) $HC1_{even}(z)$: (a) magnitude response; (b) phase response; (c) group delay; (d) impulse response; and (e) pole-zero plot in the z-plane

Figure 17 shows the characteristics of TF (47). A concise analysis of the characteristics shown in Figure 17, corresponding to TF (47), is as follows:

a. The MR corresponds to the specified values of the frequency samples at the interpolation nodes.
b. The PR is quasi-linear due to the symmetry of the interpolation nodes and the paired set of resonators.
c. The GD is constant.
d. The IR is real and symmetric.
e. The pole–zero plot in the z-plane shows that Hermitian symmetry is absent, which indicates the complex nature of TF (47); the zeros are radially symmetric.

Let us write the *low-pass* FSF TF with real coefficients of *Type I* [2], [6], [32], [36], [37], [39], [40] and with an *odd* number of resonators (five resonators):

$$HI1_{odd}(z) = (1 - z^{-26})\frac{1}{26}\left[\sum_{k=1}^{4}\frac{(-1)^k \times 2 \times 1 \times \left[cos(\frac{2\pi k}{26}) - z^{-1}\right]}{1 - 2cos(\frac{2\pi k}{26})z^{-1} + z^{-2}} + \frac{1}{1 - z^{-1}}\right]. \tag{48}$$

Figure 18 shows the characteristics of TF (48). A concise analysis of the characteristics shown in Figure 18, corresponding to TF (48), is as follows:

a. The MR corresponds to the specified values of the frequency samples at the interpolation nodes.
b. The PR is generally nonlinear; however, a nearly linear-phase region is observed within the passband.
c. The GD is nonconstant.
d. The IR is real and asymmetric.

e. The pole–zero plot in the z-plane shows that Hermitian symmetry is present, while the radial symmetry of the zeros is violated.

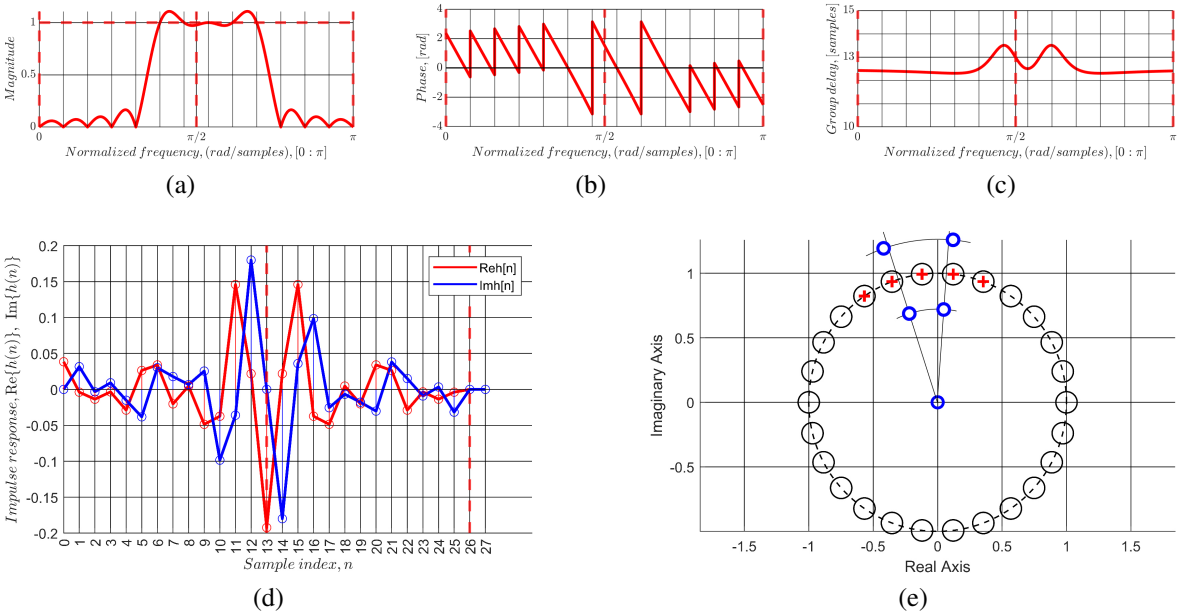

Figure 16. Characteristics of the transfer function (46) $HC2_{odd}(z)$: (a) magnitude response; (b) phase response; (c) group delay; (d) impulse response; and (e) pole-zero plot in the z-plane

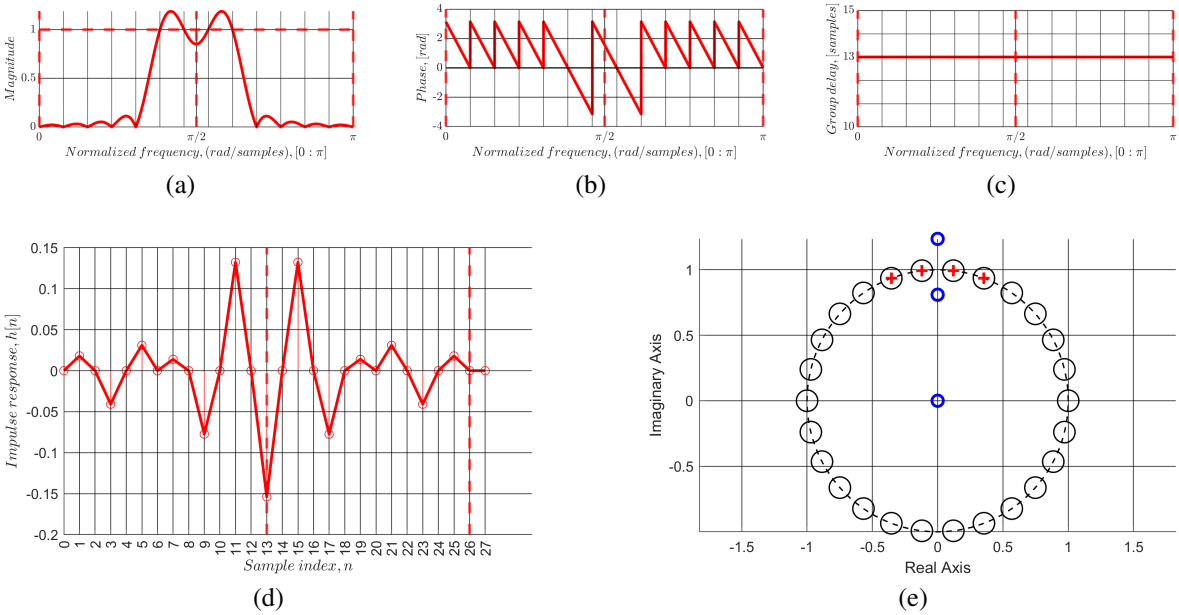

Figure 17. Characteristics of the transfer function (47) $HC2_{even}(z)$: (a) magnitude response; (b) phase response; (c) group delay; (d) impulse response; and (e) pole-zero plot in the z-plane

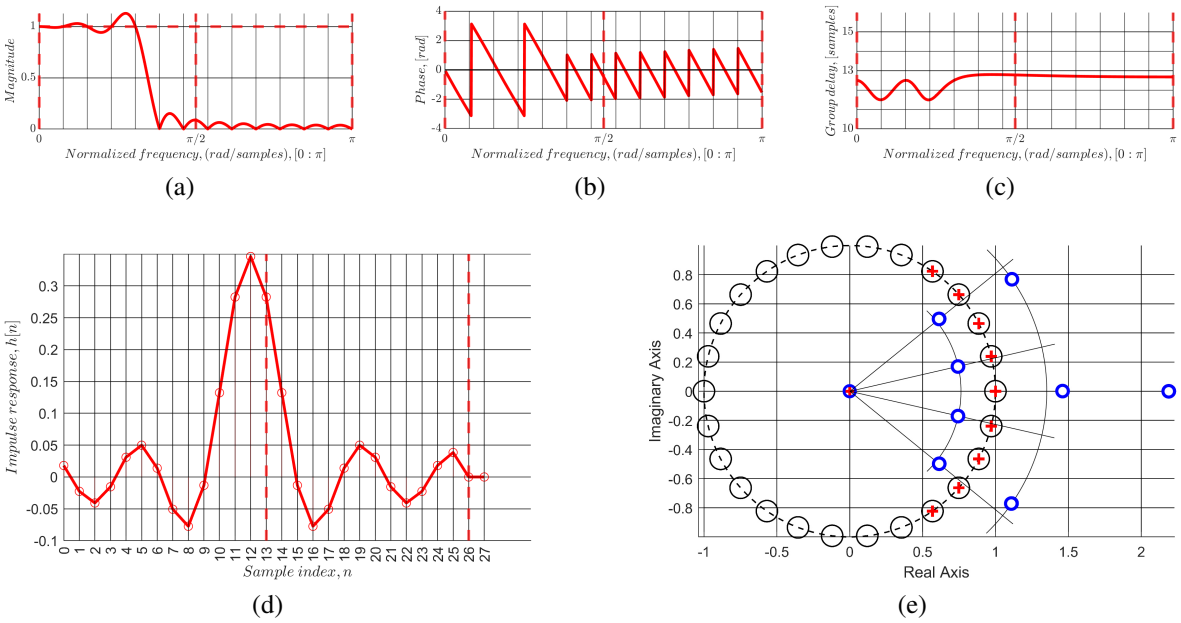

Figure 18. Characteristics of the transfer function (48) $HI1_{odd}(z)$: (a) magnitude response; (b) phase response; (c) group delay; (d) impulse response; and (e) pole-zero plot in the z-plane

Let us write the *low-pass* FSF-TF with real coefficients of *Type I* and with an *even* number of resonators (six resonators):

$$HI1_{even}(z) = (1 - z^{-26})\frac{1}{26}\left[\sum_{k=1}^{5}\frac{(-1)^k \times 2 \times 1 \times \left[cos(\frac{2\pi k}{26}) - z^{-1}\right]}{1 - 2cos(\frac{2\pi k}{26})z^{-1} + z^{-2}} + \frac{1}{1 - z^{-1}}\right]. \tag{49}$$

Figure 19 shows the characteristics of TF (49). A concise analysis of the characteristics shown in Figure 19, corresponding to TF (49), is as follows:

a. The MR corresponds to the specified values of the frequency samples at the interpolation nodes.
b. The PR is quasi-linear.
c. The GD is nonconstant, particularly within the passband region.
d. The IR is real and asymmetric.
e. The pole–zero plot in the z-plane shows that Hermitian symmetry is present, while the radial symmetry of the zeros is violated.

Let us write the *band-pass* FSF TF with real coefficients of *Type I* and with an *odd* number of resonators (five resonators):

$$HI2_{odd}(z) = (1 - z^{-26})\frac{1}{26}\left[\sum_{k=5}^{9}\frac{(-1)^k \times 2 \times 1 \times \left(cos(\frac{2\pi k}{26}) - cos\left[\frac{2\pi k}{26} - \frac{2\pi k}{26}(k + \frac{1}{2})\right] z^{-1}\right)}{1 - 2cos(\frac{2\pi k}{26})z^{-1} + z^{-2}}\right]. \tag{50}$$

Figure 20 shows the characteristics of TF (50). A concise analysis of the characteristics shown in Figure 20, corresponding to TF (50), is as follows:

a. The MR corresponds to the specified values of the frequency samples at the interpolation nodes.
b. The PR is quasi-linear.
c. The GD is nonconstant.
d. The IR is real and asymmetric.
e. The pole–zero plot in the z-plane shows that Hermitian symmetry is present, while the radial symmetry of the zeros is violated.

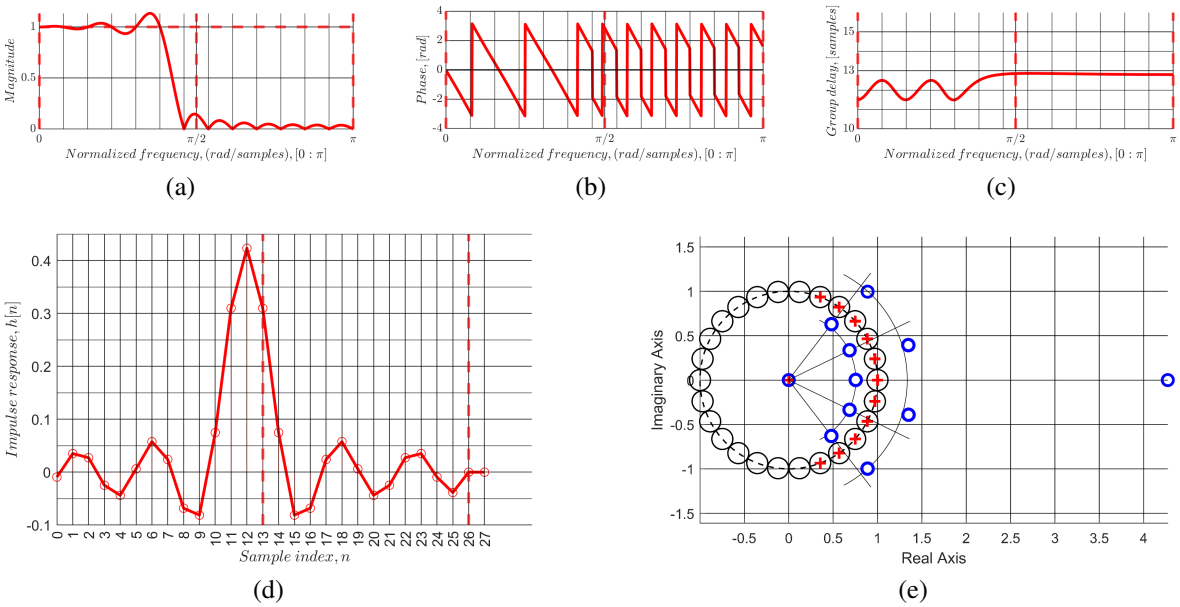

Figure 19. Characteristics of the transfer function (49) $HI1_{even}(z)$: (a) magnitude response; (b) phase response; (c) group delay; (d) impulse response; and (e) pole-zero plot in the z-plane

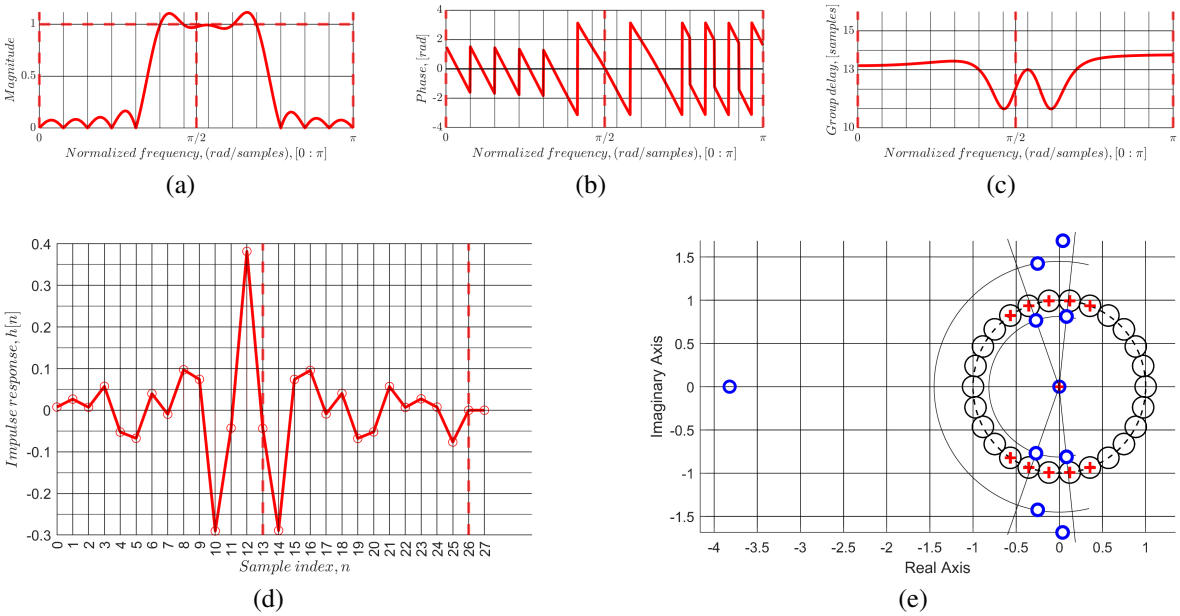

Figure 20. Characteristics of the transfer function (50) $HI2_{odd}(z)$: (a) magnitude response; (b) phase response; (c) group delay; (d) impulse response; and (e) pole-zero plot in the z-plane

Let us write the *band-pass* FSF TF with real coefficients of *Type I* and with an *even* number of resonators (four resonators):

$$HI2_{even}(z) = (1 - z^{-26})\frac{1}{26}\left[\sum_{k=5}^{8}\frac{(-1)^k \times 2 \times 1 \times (cos(\frac{2\pi k}{26}) - cos\left[\frac{2\pi k}{26} - \frac{2\pi k}{26}(k + \frac{1}{2})\right] z^{-1})}{1 - 2cos(\frac{2\pi k}{26})z^{-1} + z^{-2}}\right]. \quad (51)$$

Figure 21 shows the characteristics of TF (51). A concise analysis of the characteristics shown in Figure 21, corresponding to TF (51), is as follows:

a. The MR corresponds to the specified values of the frequency samples at the interpolation nodes.
b. The PR is quasi-linear.
c. The GD is nonconstant, particularly in the regions approaching 0 and π.
d. The IR is real and asymmetric.
e. The pole–zero plot in the z-plane shows that Hermitian symmetry is present, while the symmetry of the zeros of the resonator block is violated (Re 1 and Re –1).

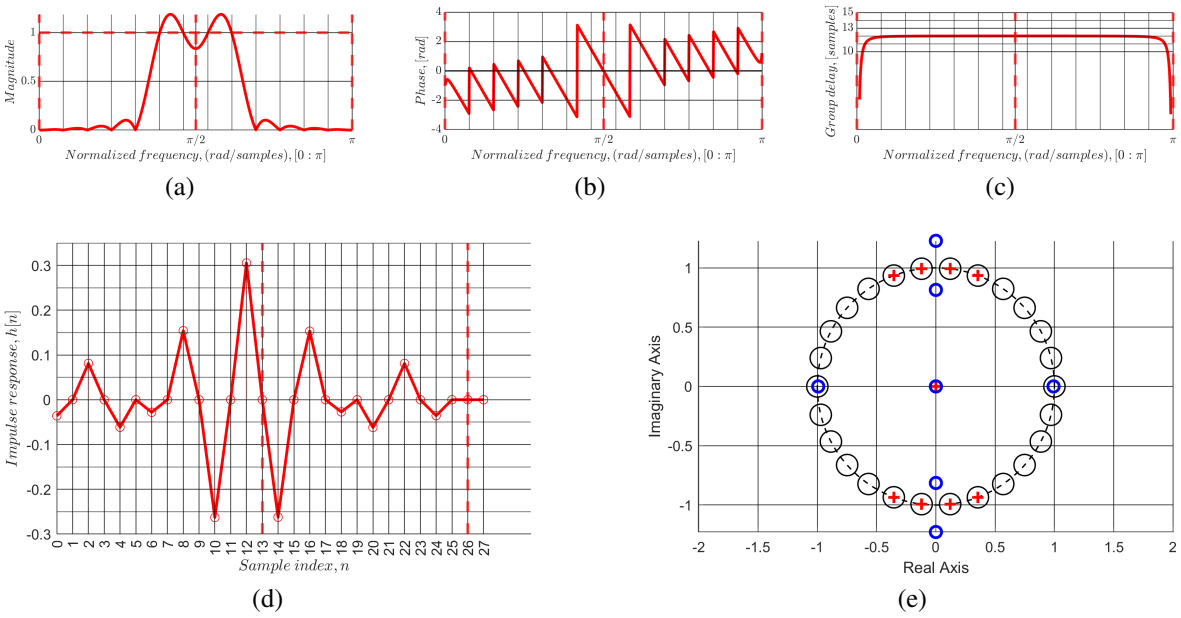

Figure 21. Characteristics of the transfer function (51) $HI2_{even}(z)$: (a) magnitude response; (b) phase response; (c) group delay; (d) impulse response; and (e) pole-zero plot in the z-plane

Let us write the *low-pass* FSF TF with real coefficients of *Type II* [1], [2], [34], [41] and with an *odd* number of resonators (seven resonators):

$$HII1_{odd}(z) = (1 - z^{-26})\frac{1}{26}\left[\sum_{k=1}^{6}\frac{(-1)^k \times 2 \times 1 \times \left[1 - cos(\frac{2\pi k}{26})z^{-1}\right]}{1 - 2cos(\frac{2\pi k}{26})z^{-1} + z^{-2}} + \frac{1 \times (1 - z^{-2})}{1 - 2z^{-1} + z^{-2}}\right]. \tag{52}$$

Figure 22 shows the characteristics of TF (52). A concise analysis of the characteristics shown in Figure 22, corresponding to TF (52), is as follows:

a. The MR corresponds to the specified values of the frequency samples at the interpolation nodes.
b. The PR is quasi-linear.
c. The GD is nonconstant.
d. The IR is real and asymmetric.
e. The pole–zero plot in the z-plane shows that Hermitian symmetry is present, while the radial symmetry of the zeros is violated.

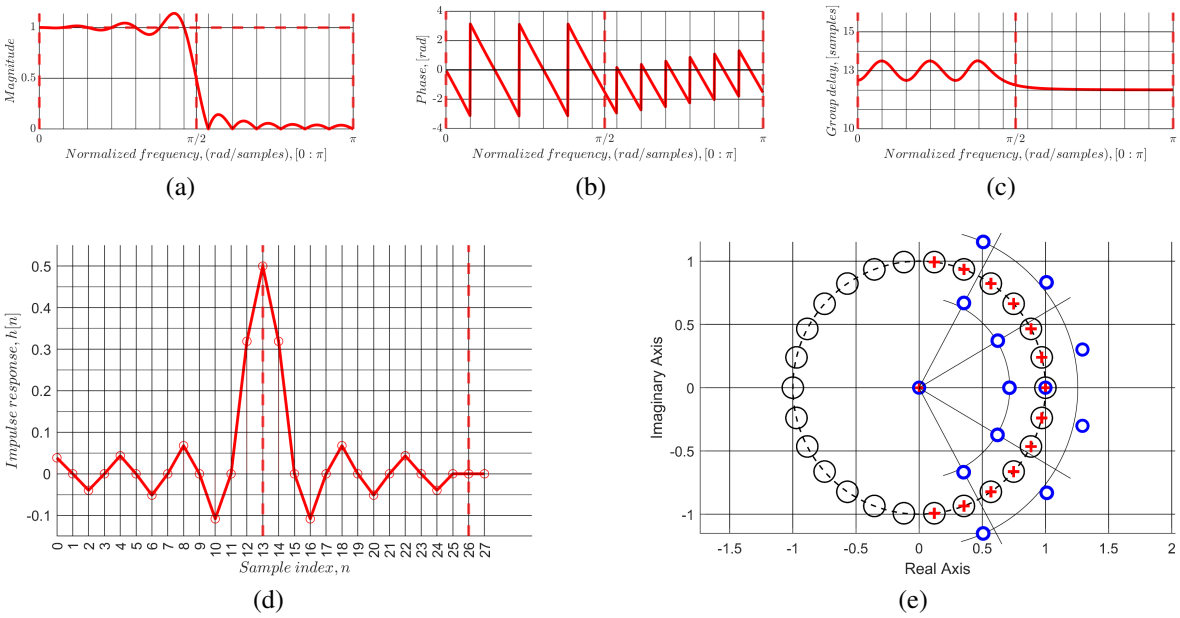

Figure 22. Characteristics of the transfer function (52) $HII1_{odd}(z)$: (a) magnitude response; (b) phase response; (c) group delay; (d) impulse response; and (e) pole-zero plot in the z-plane

Let us write the *low-pass* FSF TF with real coefficients of *Type II* and with an *even* number of resonators (six resonators):

$$HII1_{even}(z) = (1 - z^{-26})\frac{1}{26}\left[\sum_{k=1}^{5}\frac{(-1)^k \times 2 \times 1 \times \left[1 - cos(\frac{2\pi k}{26})z^{-1}\right]}{1 - 2cos(\frac{2\pi k}{26})z^{-1} + z^{-2}} + \frac{1 \times (1 - z^{-2})}{1 - 2z^{-1} + z^{-2}}\right]. \tag{53}$$

Figure 23 shows the characteristics of TF (53). A concise analysis of the characteristics shown in Figure 23, corresponding to TF (53), is as follows:

a. The MR corresponds to the specified values of the frequency samples at the interpolation nodes.
b. The PR is quasi-linear.
c. The GD is nonconstant.
d. The IR is real and asymmetric.
e. The pole–zero plot in the z-plane shows that Hermitian symmetry is present, while the radial symmetry of the zeros is violated.

Let us write the *band-pass* FSF-TF with real coefficients of *Type II* and with an *odd* number of resonators (five resonators):

$$HII2_{odd}(z) = (1 - z^{-26})\frac{1}{26}\left[\sum_{k=5}^{9}\frac{(-1)^k \times 2 \times 1 \times \left[1 - cos(\frac{2\pi k}{26})z^{-1}\right]}{1 - 2cos(\frac{2\pi k}{26})z^{-1} + z^{-2}}\right]. \tag{54}$$

Figure 24 shows the characteristics of TF (54). A concise analysis of the characteristics shown in Figure 24, corresponding to TF (54), is as follows:

a. The MR corresponds to the specified values of the frequency samples at the interpolation nodes.
b. The PR is quasi-linear.
c. The GD is nonconstant.
d. The IR is real and asymmetric.
e. The pole–zero plot in the z-plane shows that Hermitian symmetry is present, while the radial symmetry of the zeros is violated.

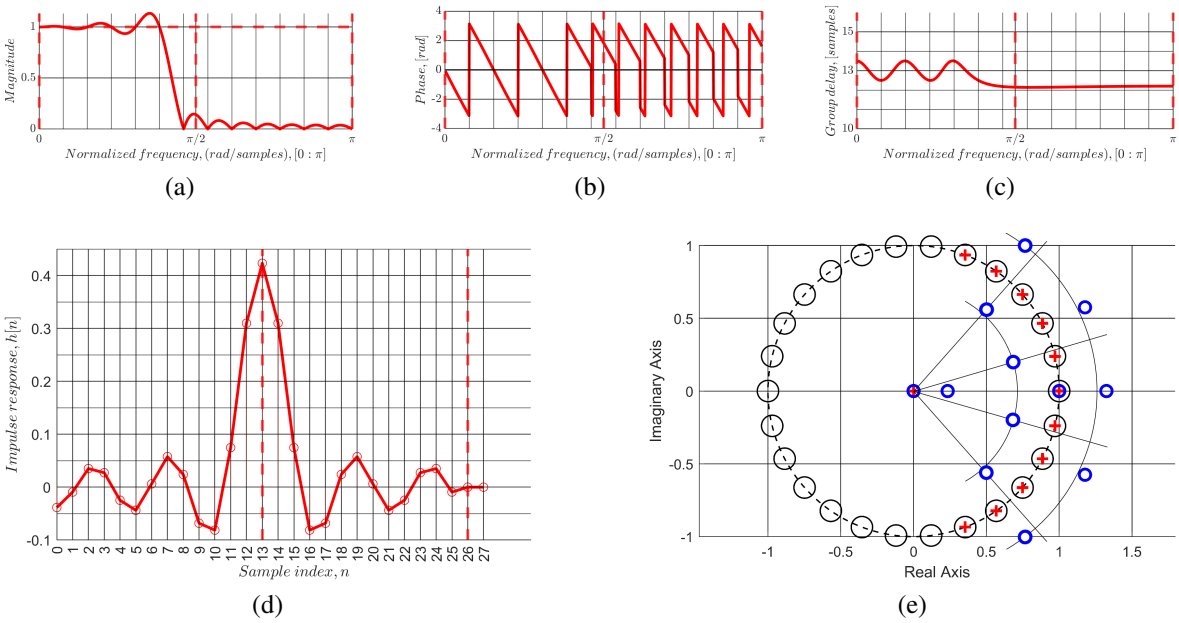

Figure 23. Characteristics of the transfer function (53) $HII1_{even}(z)$: (a) magnitude response; (b) phase response; (c) group delay; (d) impulse response; and (e) pole-zero plot in the z-plane

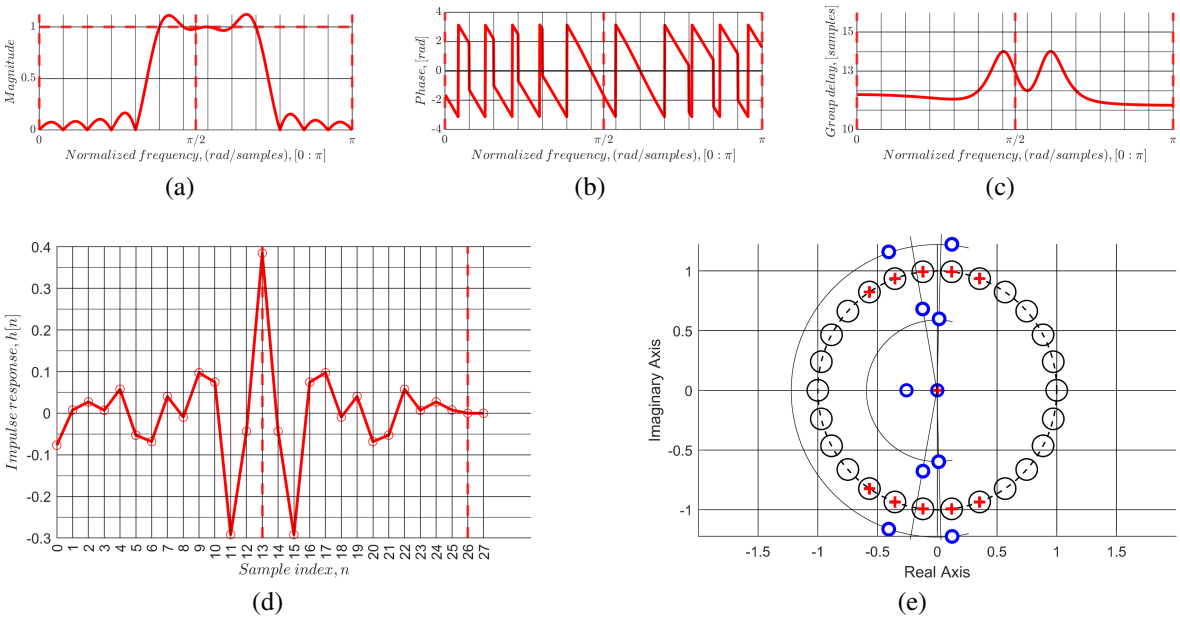

Figure 24. Characteristics of the transfer function (54) $HII2_{odd}(z)$: (a) magnitude response; (b) phase response; (c) group delay; (d) impulse response; and (e) pole-zero plot in the z-plane

Let us write the *band-pass* FSF TF with real coefficients of *Type II* and with an *even* number of resonators (four resonators):

$$HII2_{even}(z) = (1 - z^{-26})\frac{1}{26}\left[\sum_{k=5}^{8}\frac{(-1)^k \times 2 \times 1 \times \left[1 - cos(\frac{2\pi k}{26})z^{-1}\right]}{1 - 2cos(\frac{2\pi k}{26})z^{-1} + z^{-2}}\right]. \tag{55}$$

Figure 25 shows the characteristics of TF (55). A concise analysis of the characteristics shown in Figure 25, corresponding to TF (55), is as follows:

a. The MR corresponds to the specified values of the frequency samples at the interpolation nodes.
b. The PR is linear.
c. The GD is constant.
d. The IR is real and symmetric.
e. The pole–zero plot in the z-plane shows that Hermitian symmetry is present, and the radial symmetry of the zeros is not violated.

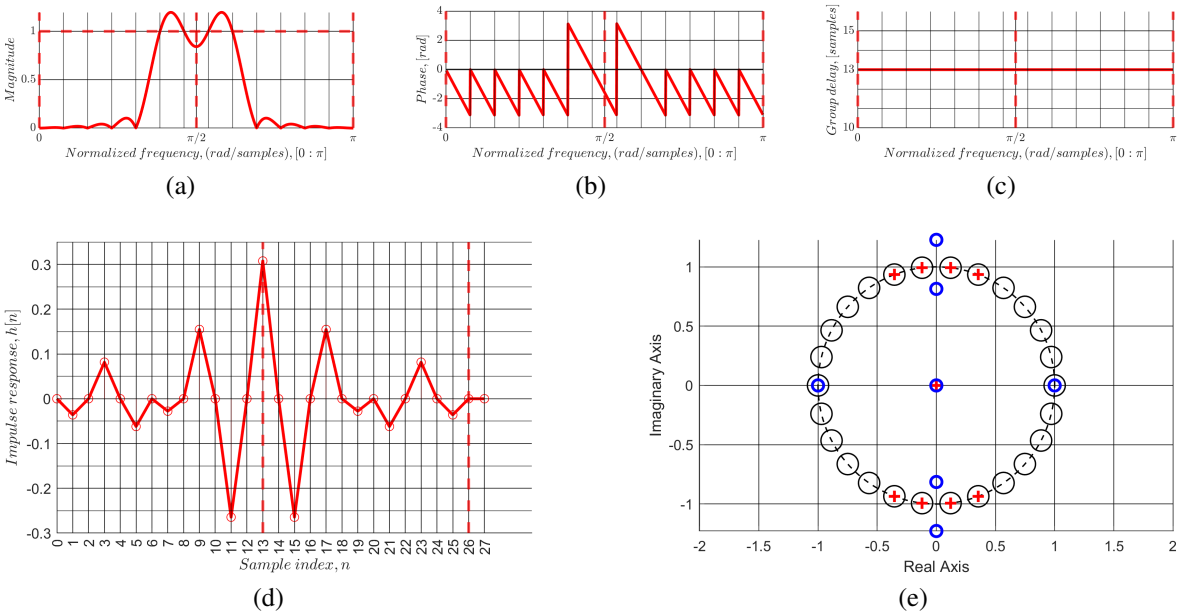

Figure 25. Characteristics of the transfer function (55) $HII2_{even}(z)$: (a) magnitude response; (b) phase response; (c) group delay; (d) impulse response; and (e) pole-zero plot in the z-plane

Let us write the *low-pass* FSF TF with real coefficients of *Type III* [2], [5], [37] and with an *odd* number of resonators (seven resonators):

$$HIII1_{odd}(z) = (1 - z^{-26})\frac{1}{26}\left[\sum_{k=1}^{6}\frac{(-1)^k \times 2 \times 1 \times cos(\frac{\pi k}{26})\left[1 - z^{-1}\right]}{1 - 2cos(\frac{2\pi k}{26})z^{-1} + z^{-2}} + \frac{1}{1 + z^{-1}}\right]. \tag{56}$$

Figure 26 shows the characteristics of TF (56). A concise analysis of the characteristics shown in Figure 26, corresponding to TF (56), is as follows:

a. The MR corresponds to the specified values of the frequency samples at the interpolation nodes.
b. The PR is quasi-linear within the passband and exhibits a fractional delay.
c. The GD is constant with a fractional delay.
d. The IR is real and asymmetric.
e. The pole–zero plot in the z-plane shows that Hermitian symmetry is present, and the radial symmetry of the zeros is not violated.

Let us write the *low-pass* FSF TF with real coefficients of Type III and with an *even* number of resonators (six resonators):

$$HIII1_{even}(z) = (1 - z^{-26})\frac{1}{26}\left[\sum_{k=1}^{5}\frac{(-1)^k \times 2 \times 1 \times cos(\frac{\pi k}{26})\left[1 - z^{-1}\right]}{1 - 2cos(\frac{2\pi k}{26})z^{-1} + z^{-2}} + \frac{1}{1 + z^{-1}}\right]. \tag{57}$$

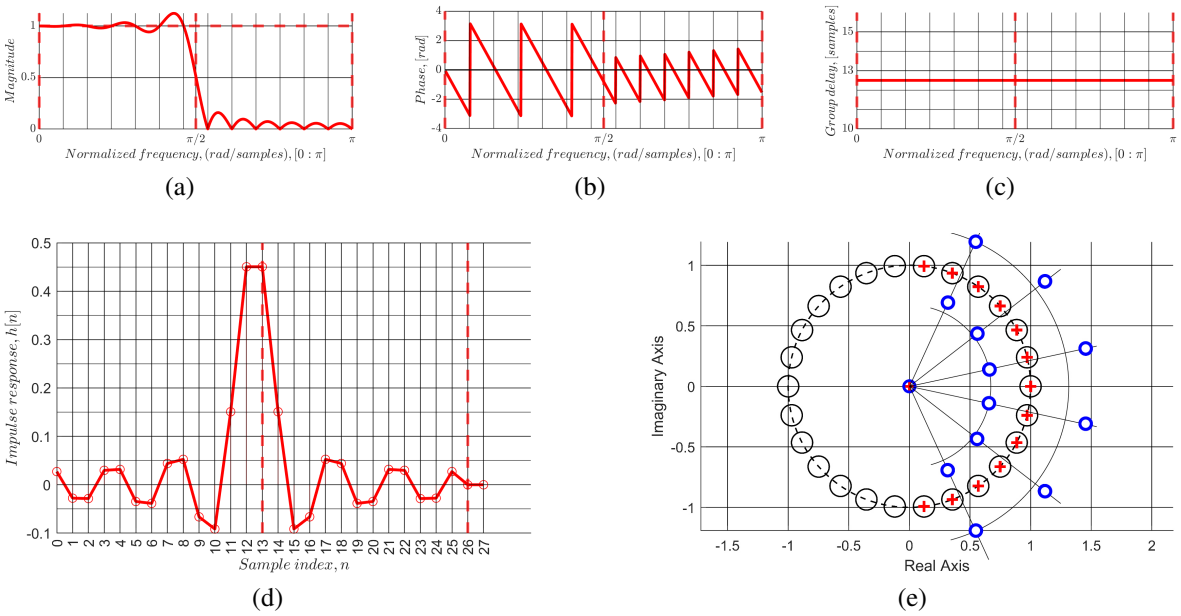

Figure 26. Characteristics of the transfer function (56) $HIII1_{odd}(z)$: (a) magnitude response; (b) phase response; (c) group delay; (d) impulse response; and (e) pole-zero plot in the z-plane

Figure 27 shows the characteristics of TF (57). A concise analysis of the characteristics shown in Figure 27, corresponding to TF (57), is as follows:

a. The MR corresponds to the specified values of the frequency samples at the interpolation nodes.
b. The PR is quasi-linear within the passband and exhibits a fractional delay.
c. The GD is constant with a fractional delay.
d. The IR is real and asymmetric.
e. The pole–zero plot in the z-plane shows that Hermitian symmetry is present, and the radial symmetry of the zeros is not violated.

Let us write the *band-pass* FSF-TF with real coefficients of *Type III* and with an *odd* number of resonators (five resonators):

$$HIII2_{odd}(z) = (1 - z^{-26})\frac{1}{26}\sum_{k=5}^{9}\frac{(-1)^k \times 2 \times 1 \times cos(\frac{\pi k}{26})\left[1 - z^{-1}\right]}{1 - 2cos(\frac{2\pi k}{26})z^{-1} + z^{-2}}. \tag{58}$$

Figure 28 shows the characteristics of TF (58). A concise analysis of the characteristics shown in Figure 28, corresponding to TF (58), is as follows:

a. The MR corresponds to the specified values of the frequency samples at the interpolation nodes.
b. The PR is quasi-linear within the passband and exhibits a fractional delay.
c. The GD is constant with a fractional delay.
d. The IR is real and asymmetric.
e. The pole–zero plot in the z-plane shows that Hermitian symmetry is present, while the radial symmetry of the zeros is violated (Re 1).

Let us write the *band-pass* FSF TF with real coefficients of *Type III* and with an *even* number of resonators (four resonators):

$$HIII2_{even}(z) = (1 - z^{-26})\frac{1}{26}\sum_{k=5}^{8}\frac{(-1)^k \times 2 \times 1 \times cos(\frac{\pi k}{26})\left[1 - z^{-1}\right]}{1 - 2cos(\frac{2\pi k}{26})z^{-1} + z^{-2}}. \tag{59}$$

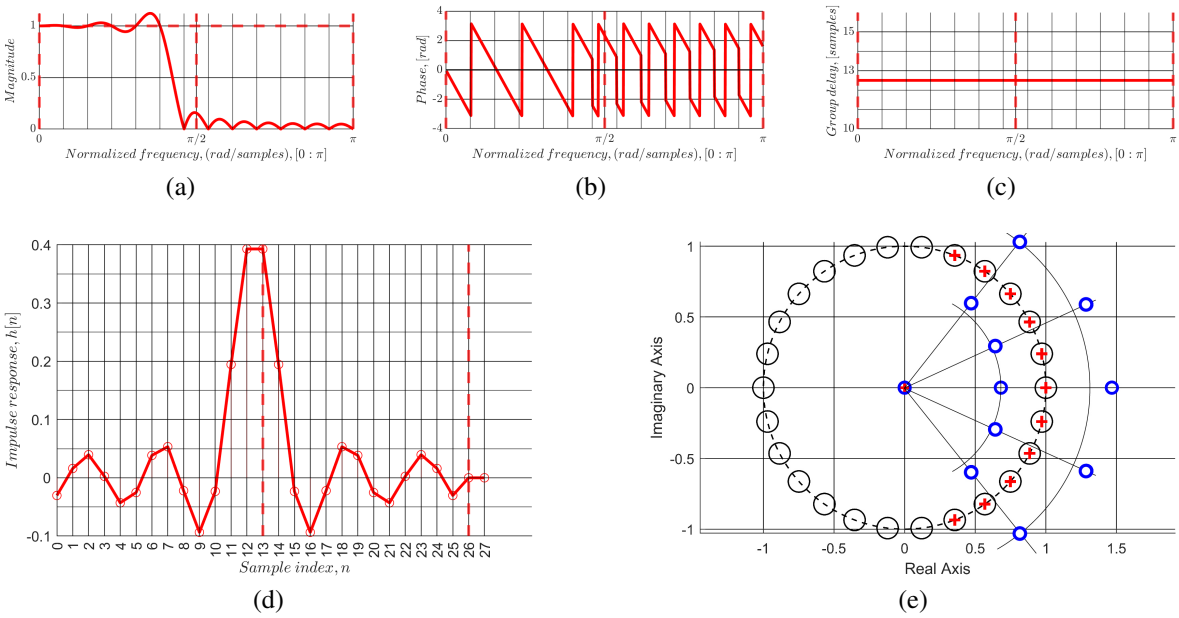

Figure 27. Characteristics of the transfer function (57) $HIII1_{even}(z)$: (a) magnitude response; (b) phase response; (c) group delay; (d) impulse response; and (e) pole-zero plot in the z-plane

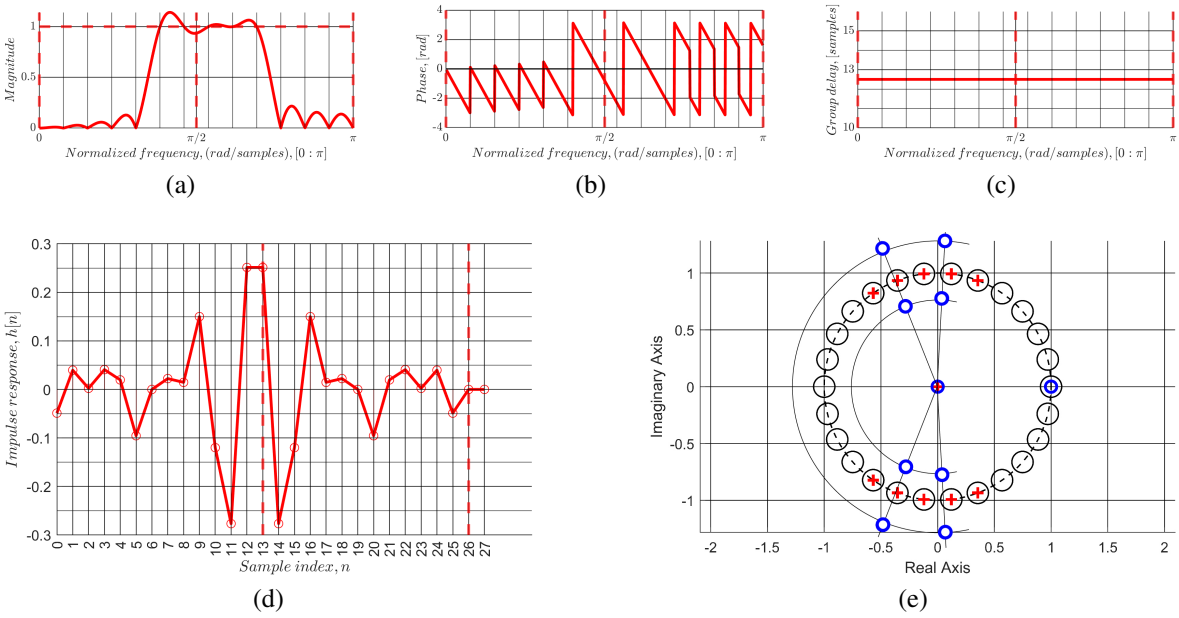

Figure 28. Characteristics of the transfer function (58) $HIII2_{odd}(z)$: (a) magnitude response; (b) phase response; (c) group delay; (d) impulse response; and (e) pole-zero plot in the z-plane

Figure 29 shows the characteristics of TF (59). A concise analysis of the characteristics shown in Figure 29, corresponding to TF (59), is as follows:

a. The MR corresponds to the specified values of the frequency samples at the interpolation nodes.
b. The PR is quasi-linear within the passband and exhibits a fractional delay.
c. The GD is constant with a fractional delay.

d. The IR is real and asymmetric.

e. The pole–zero plot in the z-plane shows that Hermitian symmetry is present, while the radial symmetry of the zeros is violated.

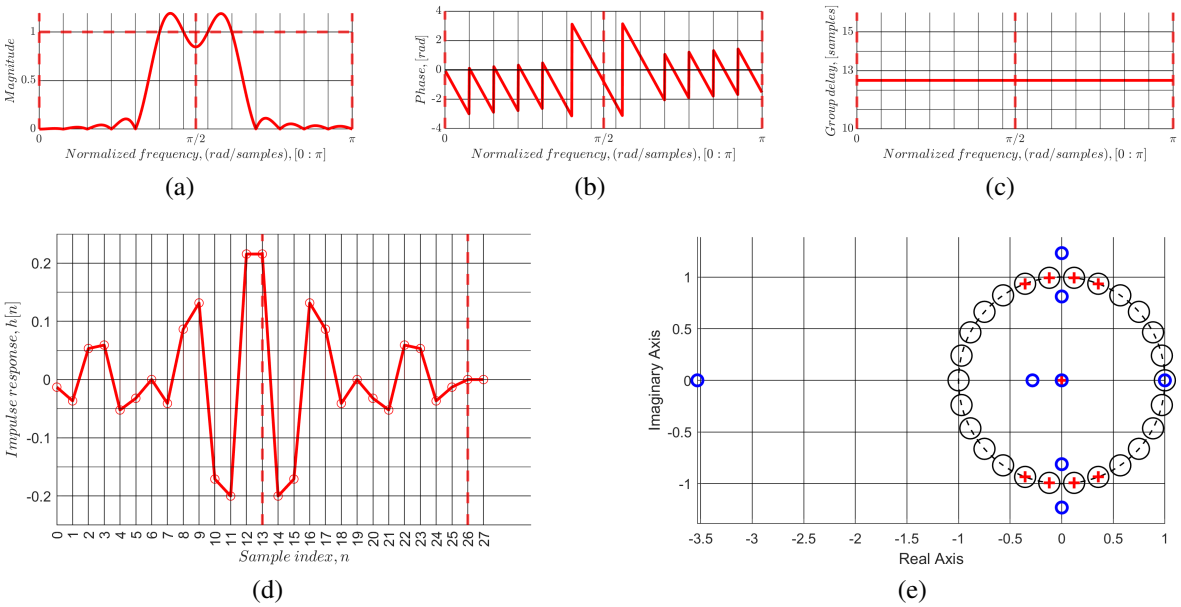

Figure 29. Characteristics of the transfer function (59) $HIII2_{even}(z)$: (a) magnitude response; (b) phase response; (c) group delay; (d) impulse response; and (e) pole-zero plot in the z-plane

Unlike the classical method, the alternative method for obtaining the FSF TF is based on the use of an analog prototype [15], [16], which exhibits favorable frequency properties in the s-plane. Its TF has the following general form:

$$T_l(s) = \frac{\sum_{kl=r+1}^{r+\frac{n}{2}} (a_k \frac{s^2}{s^2+\omega_{kl}^2})}{1 + \sum_{k=r+1}^{r+\frac{n}{2}} (b_k \frac{s}{s^2+\omega_k^2})}. \tag{60}$$

Based on TF (60), efficient filter banks with near-linear PR are realized [16]. The electrical circuit of the analog prototype (Figure 1) represents a multichannel configuration with one input and l-outputs. It consists of parallel-connected LC-resonators. Each resonator, at its resonant frequency, shunts the signal and thereby forms a zero of the MR. If a weighted signal (sample) is taken from the midpoint of the LC-resonator, a specific fragment of the MR of the filter's passband is formed. The set of such samples shapes the passband of the electrical filter. The number of resonators that realize samples for the l-th output is small compared to the total number of resonators that form the zeros. In general, the greater the number of resonators in the circuit, the closer its behavior approaches a linear phase for each l-th output of the multichannel system. Accordingly, the group delay will be identical for all l-th outputs of the filter bank.

The requirement of approximating an absolutely linear PR over the entire operating frequency band of the analog filter was formulated. As a result of the analysis performed (section 2 of this paper), the ideal TF with an absolutely linear PR was obtained:

$$T(s) = \frac{\sum_{k-1}^{\frac{n}{2}} (a_k \frac{s^2}{s^2+\omega_k^2})}{\frac{e^{\tau s}}{cosh\tau s}} = \sum_{k-1}^{\frac{n}{2}} (a_k \frac{s^2}{s^2+\omega_k^2}) cosh\tau s e^{-\tau s} = \sum_{k-1}^{\frac{n}{2}} (a_k \frac{s^2}{s^2+\omega_k^2})(1 \pm e^{-\tau s}). \tag{61}$$

Theoretically, the ideal analog implementation of TF (61) presumes an electrical circuit of a multipole network comprising an infinite number of LC-resonators, in contrast to the finite number of resonators in TF (60). The total finite number of resonators in TF (60) is determined by its denominator: $1 + \sum_{k=r+1}^{r+\frac{n}{2}} (b_k \frac{s}{s^2+\omega_k^2})$.

An infinite number of LC-resonators of TF (61), if no signal is taken from their midpoints, shunt the signal at their resonant frequencies and thereby produce an infinite number of zeros of TF (61) (Figure 2(b)). And the numerator of TF (61), represented by the polynomial: $\sum_{k=1}^{\frac{n}{2}}(a_k\frac{s^2}{s^2+\omega_k^2})$, produces the specified number of poles (Figure 2(a)). When the frequencies of a zero and a pole coincide, an interpolation node of the MR is formed. It is important to note that the interpolation node is formed jointly by the zero and the pole of the TF (61).

When examining the numerator and denominator of TF (60), one can notice an interesting transformation of the TF denominator into the numerator. When the requirement for an absolutely linear PR of the filter is satisfied, the denominator of TF (60) is transformed into the factor: $\left(1 \pm e^{-2\tau s}\right)$ in the numerator of TF (61). It is also important to note that the truncation of the denominator in the ideal TF (61) does not occur, in contrast to the truncation of the denominator in the physically implemented TF (60). It is well known that the truncation of the denominator of the TF filter causes distortion of its PR.

After performing the transformation of TF (61) from the s-plane to the z-plane (section 3 of this paper), the following TF was obtained:

$$H_l(z) = (1 - z^{-m})(1 - z^{-1})^2 \sum_{kl}^{nl} \frac{A_{kl}^*}{1 + b_{1kl}z^{-1} + z^{-2}}. \tag{62}$$

TF (62) was modified in order to eliminate the deformation of the FR that arose due to the application of the bilinear z-transformation to the polynomial: $\sum_{k=1}^{\frac{n}{2}}\left(a_k\frac{s^2}{s^2+\omega_k^2}\right)$. This polynomial implements a resonator. It is important to note that the deformation of the frequency response occurred in the amplitude of the resonators (section 4 of this paper, Figure 4). Considering that the samples are taken at equally spaced frequencies, the deformation of the frequency scale does not occur. It is not necessary to apply frequency pre-warping when designing an FSF based on an analog prototype.
The FSF TF assumes the following form:

$$H(z) = (1 - z^{-m})\frac{1}{m}\sum_{k=1}^{n} \frac{A_k(1 - z^{-2})}{1 + b_{1k}z^{-1} + z^{-2}}. \tag{63}$$

The polynomial: $\sum_{k=1}^{n}\left(\frac{A_k\left(1-z^{-2}\right)}{1+b_{1k}z^{-1}+z^{-2}}\right)$ (63) implements the resonators. Such a form of the TF resonator differs from all known classical types of TF resonators in FSF. In practical implementation of TF (63), it is advisable to take the factor $\left(1 - z^{-2}\right)$ outside the polynomial. This factor is common to all resonators of the FSF TF (63). Let us express the FSF TF in the following form [2], [25]:

$$H(z) = (1 - z^{-m})\frac{1}{m}(1 - z^{-2})\sum_{k=1}^{n} \frac{A_k}{1 + b_{1k}z^{-1} + z^{-2}}. \tag{64}$$

The weighting coefficients A_k of TF (64) are frequency-independent over the entire operating band of the filter and are determined by the following expression:

$$A_k = (-1)^{q+1}H(jx_k).$$

Using an analytical approach based on an ideal analog prototype (the indirect method), an alternative FSF TF (64) [25] was obtained. The obtained FSF TF is then employed in the direct synthesis method, without reference to the analog prototype, by means of interpolation on the frequency grid. The alternative method for obtaining the FSF TF fundamentally differs from the classical one. For comparison with the characteristics of the main classical types of FSF TF, let us briefly consider the characteristics of TF FSF (64), which was obtained by an alternative method.

Let us define the following conditions for the alternative FSF TF (64); they are analogous to the conditions for the basic classical types of FSF TF:

- the order of the comb filter is m = 26;
- all weighting coefficients of TF (64) are chosen to be equal to unity;

- in the transition band, the weighting coefficients are not applied.

Let us write the *low-pass* FSF TF with real coefficients of the alternative FSF TF [2], [25] and with an *odd* number of resonators (seven resonators):

$$HA1_{odd}(z) = (1 - z^{-26})\frac{1}{26}(1 - z^{-2})\left[\sum_{k=1}^{6}\frac{(-1)^k \times 1}{1 - cos(\frac{2\pi k}{26})z^{-1} + z^{-2}} + \frac{1/2}{1 - z^{-1} + z^{-2}}\right]. \quad (65)$$

Figure 30 shows the characteristics of TF (65). A concise analysis of the characteristics shown in Figure 30, corresponding to TF (65), is as follows:

a. The MR corresponds to the specified values of the frequency samples at the interpolation nodes.
b. The PR is linear.
c. The GD is constant.
d. The IR is real and symmetric.
e. The pole–zero plot in the z-plane shows that Hermitian symmetry is present, and the radial symmetry of the zeros is preserved.

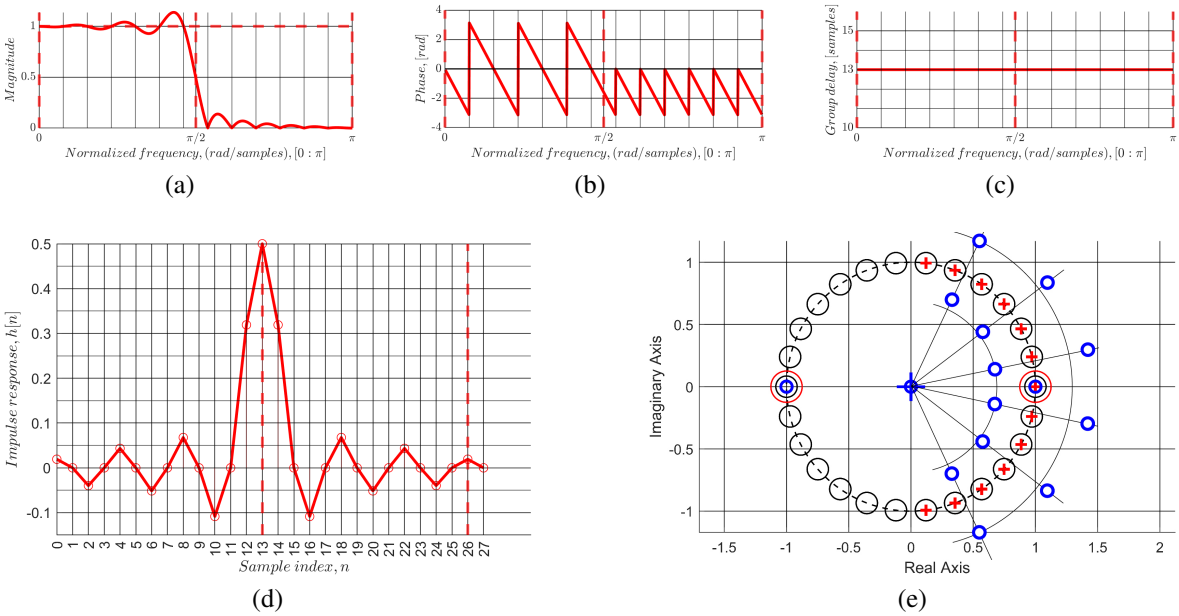

Figure 30. Characteristics of the transfer function (65) $HA1_{odd}(z)$: (a) magnitude response; (b) phase response; (c) group delay; (d) impulse response; and (e) pole-zero plot in the z-plane

Let us write the *low-pass* FSF TF with real coefficients of the alternative FSF TF and with an *even* number of resonators (six resonators):

$$HA1_{even}(z) = (1 - z^{-26})\frac{1}{26}(1 - z^{-2})\left[\sum_{k=1}^{5}\frac{(-1)^k \times 1}{1 - cos(\frac{2\pi k}{26})z^{-1} + z^{-2}} + \frac{1/2}{1 - z^{-1} + z^{-2}}\right]. \quad (66)$$

Figure 31 shows the characteristics of TF (66). A concise analysis of the characteristics shown in Figure 31, corresponding to TF (66), is as follows:

a. The MR corresponds to the specified values of the frequency samples at the interpolation nodes.
b. The PR is linear.
c. The GD is constant.
d. The IR is real and symmetric.

e. The pole–zero plot in the z-plane shows that Hermitian symmetry is present, and the radial symmetry of the zeros is preserved.

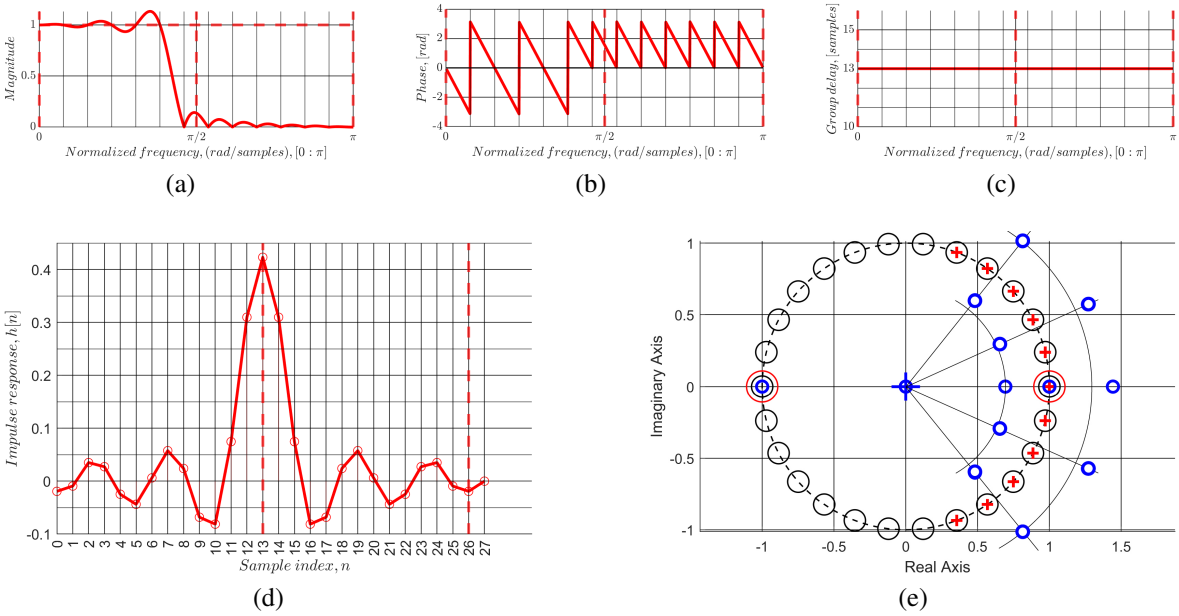

Figure 31. Characteristics of the transfer function (66) $HA1_{even}(z)$: (a) magnitude response; (b) phase response; (c) group delay; (d) impulse response; and (e) pole-zero plot in the z-plane

Let us write the *band-pass* FSF TF with real coefficients of the alternative FSF TF and with an *odd* number of resonators (five resonators):

$$HA2_{odd}(z) = (1 - z^{-26})\frac{1}{26}(1 - z^{-2})\sum_{k=5}^{9}\frac{(-1)^k \times 1}{1 - 2cos(\frac{2\pi k}{26})z^{-1} + z^{-2}}. \tag{67}$$

Figure 32 shows the characteristics of TF (67). A concise analysis of the characteristics shown in Figure 32, corresponding to TF (67), is as follows:

a. The MR corresponds to the specified values of the frequency samples at the interpolation nodes.
b. The PR is linear.
c. The GD is constant.
d. The IR is real and symmetric.
e. The pole–zero plot in the z-plane shows that Hermitian symmetry is present, and the radial symmetry of the zeros is preserved.

Let us write the *band-pass* FSF TF with real coefficients of the alternative FSF TF and with an *even* number of resonators (four resonators):

$$HA2_{even}(z) = (1 - z^{-26})\frac{1}{26}(1 - z^{-2})\sum_{k=5}^{8}\frac{(-1)^k \times 1}{1 - 2cos(\frac{2\pi k}{26})z^{-1} + z^{-2}}. \tag{68}$$

Figure 33 shows the characteristics of TF (68). A concise analysis of the characteristics shown in Figure 33, corresponding to TF (68), is as follows:

a. The MR corresponds to the specified values of the frequency samples at the interpolation nodes.
b. The PR is linear.
c. The GD is constant.
d. The IR is real and symmetric.

e. The pole–zero plot in the z-plane shows that Hermitian symmetry is present, and the radial symmetry of the zeros is preserved.

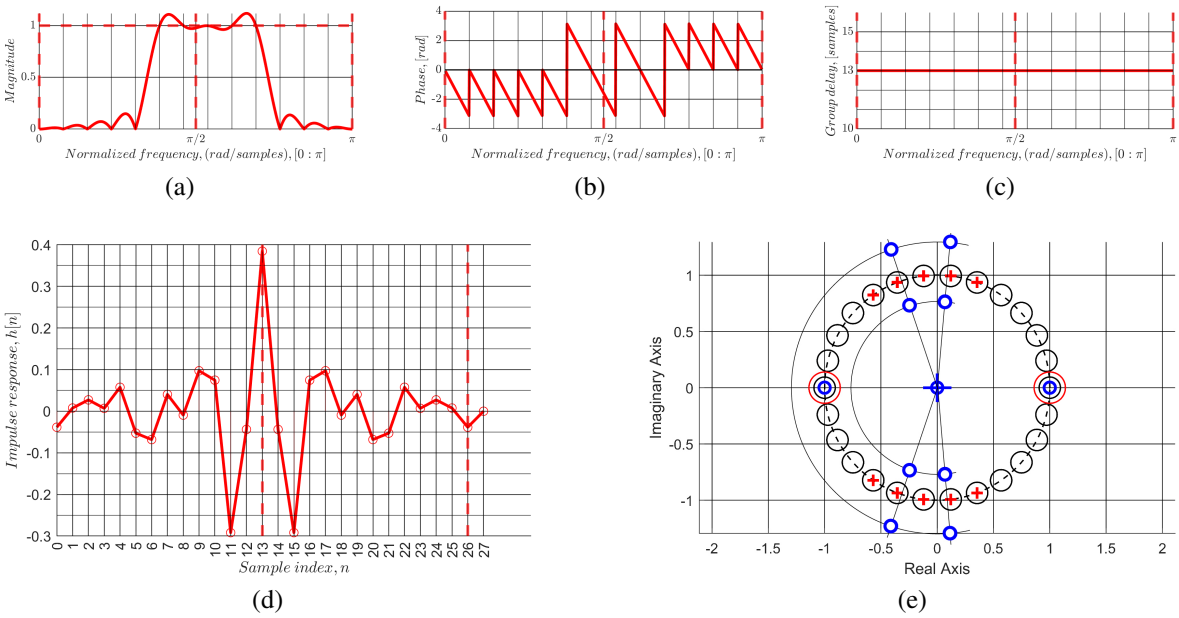

Figure 32. Characteristics of the transfer function (67) $HA2_{odd}(z)$: (a) magnitude response; (b) phase response; (c) group delay; (d) impulse response; and (e) pole-zero plot in the z-plane

Based on the above analysis, it can be concluded that in order to obtain PR-filter linearity, the following conditions must be satisfied.

For classical FSF TF:

The basic condition of PR-filter linearity requires that frequency samples must satisfy the complex-conjugate symmetry property. Consequently, the IR is real and symmetric (or antisymmetric). Accordingly, the zeros and poles of the TF are located symmetrically with respect to the real axis of the z-plane. All coefficients of the equivalent realization are real in this case.

However, according to the calculated characteristics, the classical FSF TF does not always satisfy *the basic condition of PR-filter linearity*.

For the alternative FSF TF:

In the s-plane, *the boundary condition of PR-filter linearity* requires that the Hurwitz polynomial $V(s)$ (the denominator of the TF) satisfy the relation involving the functions $cosh\tau s + sinh\tau s$. When this ideal analog prototype is used for the transformation into the z-plane, the resulting alternative FSF TF inherits the properties of the ideal analog prototype. In the subsequent synthesis, this TF is employed in the direct FSF synthesis method without referring to the analog prototype. The FSF realized on the basis of the alternative transfer function is always linear-phase. Moreover, the alternative FSF TF always satisfies the above-mentioned *basic condition of PR-filter linearity*.

Thus, the analytical method based on the use of an ideal analog prototype is, in essence, an independent and direct method for the synthesis of digital filters (the alternative frequency-sampling method). It differs from the classical frequency-sampling method not merely by a sequence of computational steps, but by the very principle of TF formation.

It should be emphasized that *the boundary condition of PR-filter linearity* is determined already at the stage of analytical synthesis of the alternative FSF TF. In other words, the PR linearity is inherently embedded in the structure of the alternative FSF TF.

Due to the preservation of the prototype's phase properties, the alternative method provides better phase characteristics than the classical designs based on the frequency-sampling method. At the same time, the alternative FSF TF retains the ability for precise control over the filter's frequency characteristics.

The above concise analysis of the characteristics of the classical FSF TF and the alternative FSF TF clearly demonstrates the advantages of the alternative FSF TF compared with the classical one.

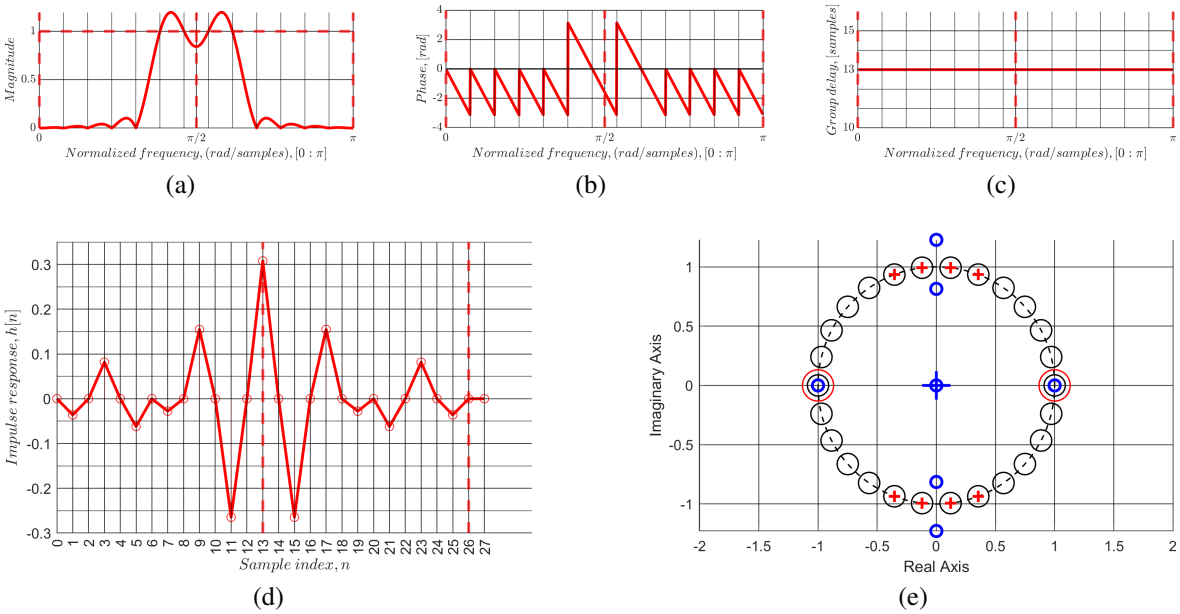

Figure 33. Characteristics of the transfer function (68) $HA2_{even}(z)$: (a) magnitude response; (b) phase response; (c) group delay; (d) impulse response; and (e) pole-zero plot in the z-plane

8. CONCLUSION

We conducted a theoretical review of the derivation of a modified (alternative) TF for a linear-phase FIR FSF with a recursive implementation and real coefficients. To derive the modified (alternative) TF FSF, a novel original approach was applied using an ideal analog prototype with a linear PR. This subsequently allowed us to successfully apply accumulated knowledge regarding solving the analog prototype approximation problem in FSF design. The analog prototype exhibits similar FR properties to those of the FSF FR. The obtained TF FSF is computationally very efficient. It has the minimum necessary number of coefficients. Consequently, the TF FSF requires a relatively small number of multiplication operations for its implementation. The article demonstrates how an analytical expression was derived for calculating the weighting coefficients of the modified TF FSF by employing interpolation at frequencies where zeros and poles of the TF coincide. As a result of the TF modification, the values of its weighting coefficients become independent of frequency across the entire operational frequency range of the filter. The MR at the interpolation node equals the specified value of the corresponding weighting coefficient A_k.

The modified TF FSF with real coefficients, unlike the traditional TF FSF, acquires a number of useful properties: $Interpolation\ convenience$. Due to the fact that the values of the weighting coefficients A_k of the modified TF are equal to the magnitude response at the interpolation nodes (where the zeros and poles of the TF coincide), it becomes convenient to use the interpolation method when determining the initial solution for the approximation problem. $Enhanced\ passband\ control$. The weighting coefficients A_k in the passband, under the requirement of forming a flat FSF MR, are preferably chosen equal to one, which increases the efficiency of the filter and simplifies its implementation. If necessary, it is possible to approximate the MR in the filter's passband according to a given proximity criterion (for example, based on the Chebyshev approximation criterion). In this case, an equiripple approximation of the MR in the passband can be obtained, but the weighting coefficients A_k will not be equal to one. $High\ suitability\ for\ FSF\ banks$. FSFs based on a modified TF are efficient for implementing high-performance FSF banks. If a symmetric solution to the FSF approximation problem is calculated with respect to the central frequency value $\pi/2$ of the operating range, this solution can be applied to generate similar filters MR across the entire frequency range. In this case, the weighting coefficients will be the same (identical) for all outputs of the filter bank. This approach reduces the time required to

solve the approximation problem separately for each output of the filter bank and simplifies its implementation. *Sliding and stepped frequency operation*. It is evident that the identity property enables the implementation of sliding or stepped frequency modes of FSF operation. The minimum frequency step corresponds to the spacing between the zeros of the comb filter. *Ripple control*. The transitional weighting coefficients of the modified TF FSF provide effective control of the ripple of the MR in the passbands and stopbands. Ripples at the edges of the passband can be effectively suppressed by selecting the optimal value of the so-called Gibbs coefficient, G. *Implementation simplicity*. The modified TF FSF consists of simple components: a comb filter and guaranteed stable second-order resonators with real coefficients. These components are well-studied and possess favorable properties for filter implementation. Therefore, the implementation of a modified TF FSF is not complex. The use of the improved Rybka-Lyons FSF block diagram significantly enhances the computational efficiency of FSF and FSF banks. The provided table of calculated optimal weighting coefficient values, along with the attenuation characteristic graph of the modified FSF, allows for a comparison of its effectiveness with other similar digital filters. For example, with Parks–McClellan FIR filters.

The results of a comparative analysis of the classical and alternative FSF TF demonstrate that, unlike the classical structures, the alternative TF consistently maintains a linear-phase response.

For the successful advancement of FSF design technology, it is necessary to address the challenges outlined in the introduction of this article. The approaches to resolving these issues will be presented in subsequent studies. An important research direction in FSF design is the investigation of synthesis techniques based on nonuniform frequency sampling. For this purpose, structural implementation schemes using the Lagrange interpolation formula can be considered. When the precision of filter coefficient representation is limited, such structures provide additional benefits. Moreover, the application of the Lagrange structure enables optimization of the order of the implemented filter.

ACKNOWLEDGMENTS

We are grateful to Associate Professor Valery Sobolev for setting the research task and providing scientific guidance, promising ideas, and support. In loving memory.

We are also grateful to Professor Ivan Trifonov for insightful scientific consultations and discussions on ways to overcome challenging issues. In loving memory.

Special thanks to Richard G. Lyons, author of outstanding books on DSP, for engaging discussions regarding the properties of FSFs.

FUNDING INFORMATION

Authors state no funding involved.

AUTHOR CONTRIBUTIONS STATEMENT

This journal uses the Contributor Roles Taxonomy (CRediT) to recognize individual author contributions, reduce authorship disputes, and facilitate collaboration.

Name of Author	C	M	So	Va	Fo	I	R	D	O	E	Vi	Su	P	Fu
Serhii Rybka	✓	✓		✓	✓				✓	✓		✓		
Ivan Varava		✓	✓	✓	✓	✓		✓	✓		✓			

C : **C**onceptualization
M : **M**ethodology
So : **So**ftware
Va : **Va**lidation
Fo : **Fo**rmal Analysis
I : **I**nvestigation
R : **R**esources
D : **D**ata Curation
O : Writing - **O**riginal Draft
E : Writing - Review & **E**diting
Vi : **Vi**sualization
Su : **Su**pervision
P : **P**roject Administration
Fu : **Fu**nding Acquisition

CONFLICT OF INTEREST STATEMENT

Authors state no conflict of interest.

ETHICAL APPROVAL

Not applicable.

DATA AVAILABILITY

The data that support the findings of this study are contained within the article.

REFERENCES

[1] B. Gold and C. M. Rader, *Digital Processing of Signals*, New York, NY, USA: McGraw-Hill, 1969.

[2] R. Lyons, *Understanding Digital Signal Processing*, 3rd ed. Upper Saddle River, NJ, USA: Prentice Hall, 2011.

[3] L. R. Rabiner, B. Gold, and M. McGonegal, "An approach to the approximation problem for nonrecursive digital filters," *IEEE Transactions on Audio and Electroacoustics*, vol. 18, no. 2, pp. 83–106, Jun. 1970, doi: 10.1109/TAU.1970.1162092.

[4] J. H. McClellan and T. W. Parks, "A unified approach to the design of optimum FIR linear-phase digital filters," *IEEE Transactions on Circuit Theory*, vol. 20, no. 6, pp. 697-701, Nov. 1973, doi: 10.1109/TCT.1973.1083764.

[5] P. A. Stubberud and C. T. Leondes, "The design of frequency sampling filters by method of Lagrange multipliers," *IEEE Transactions on Circuits and Systems II: Analog and Digital Signal Processing*, vol. 40, no. 1, pp. 51–54, Jan. 1993, doi: 10.1109/82.215360.

[6] S. P. Harris and E. C. Ifeachor, "Automatic design of frequency sampling filters by hybrid genetic algorithm techniques," *IEEE Transactions on Signal Processing*, vol. 46, no. 12, pp. 3304–3314, Dec. 1998, doi: 10.1109/78.735305.

[7] W.-P. Huang, L.-F. Zhou, and J.-X. Qian, FIR filter design: frequency sampling filters by particle swarm optimization algorithm, *Proceedings of 2004 International Conference on Machine Learning and Cybernetics (IEEE Cat. No.04EX826)*, Shanghai, China, 2004, pp. 2322-2327 vol.4, doi: 10.1109/ICMLC.2004.1382187.

[8] R. Y. Belorutsky, M. V. Oreshkin, and I. S. Savinykh, "The analytical approach for designing bandpass FIR filters by frequency sampling method," in *2017 International Multi-Conference on Engineering, Computer and Information Sciences (SIBIRCON)*, Novosibirsk, Russia, 2017, pp. 239-244, doi: 10.1109/SIBIRCON.2017.8109879.

[9] L. Jiang, H. Zhang, S. Cheng, H. Lv, and P. Li, "An overview of FIR filter design in future multicarrier communication systems," *Electronics*, vol. 9, no. 4, pp. 1-34, 2020, doi: 10.3390/electronics9040599.

[10] A. A. Hoshu, L. Wang, S. Ansari, A. Sattar, and M. H. A. Bilal, "System identification of heterogeneous multirotor unmanned aerial vehicle," *Drones*, vol. 6, no. 10, pp. 1-22, Oct. 2022, doi: 10.3390/drones6100309.

[11] P. Stubberud, "Analog frequency sampling filters," in *Proceedings of the 30th International Conference on Systems Engineering (ICSEng) 2023*, Cham, Switzerland: Springer, 2023, vol. 761, pp. 195–204, doi: 10.1007/978-3-031-40579-2_19.

[12] P. Stubberud, "An optimization method for designing analog frequency sampling filters," in *Models and Methods for Systems Engineering*, Cham, Switzerland: Springer, Jan. 2025, pp. 263–275, doi: 10.1007/978-3-031-76440-0_21.

[13] L. R. Rabiner and B. Gold, *Theory and Application of Digital Signal Processing*, Englewood Cliffs, NJ, USA: Prentice Hall, 1975.

[14] G. C. Temes and S. K. Mitra, *Modern Filter Theory and Design*, New York, NY, USA: Wiley, 1973.

[15] L. A. Babkova and A. F. Beletsky, "New principles of designing comb electric filters," *Voprosy Radioelektroniki, Series: Theory of Signal Transmission*, no. 9, pp. 3–7, 1975.

[16] L. A. Babkova, "Research of the new principles of designing comb electric filters," Ph.D. dissertation, Leningrad Electrotechnical Institute of Communications, Leningrad, USSR, 1976.

[17] A. F. Beletsky, *Theoretical Foundations of Wire Communication, Part. III: Synthesis of Reactive Four-Pole Networks and Electric Filters*, M., USSR: Svyazizdat, 1959.

[18] A. F. Beletsky, *Fundamentals of the Theory of Linear Electric Circuits*, M., USSR: Svyaz, 1966.

[19] I. I. Trifonov, *Synthesis of Reactive Networks with Prescribed Phase Characteristics*, M., USSR: Svyaz, 1969.

[20] I. I. Trifonov, *Calculation of Electronic Circuits with Prescribed Frequency Characteristics*, M., USSR: Radio i Svyaz, 1988.

[21] B. N. Pshenichny and Yu. M. Danilin, *Numerical Methods in Extremal Problems*, M., USSR: Nauka, 1975.

[22] I. N. Bronshtein and K. A. Semendyayev, *Handbook of Mathematics for Engineers and Students of Technical Colleges*, M., USSR: Nauka, 1981.

[23] I. S. Gradshteyn and I. M. Ryzhik, *Tables of Integrals, Sums, Series, and Products*, M., USSR: Nauka, 1971.

[24] G. A. Korn and T. M. Korn, *Mathematical Handbook for Scientists and Engineers: Definitions, Theorems, and Formulas for Reference and Review*, 2nd rev. ed. New York, USA: McGraw-Hill, 1968.

[25] S.V. Rybka and S.N. Mansurov, "Recursive Digital Filters with Linear Phase-Frequency Response," *Radioelectronics and Communications (Iz. VUZ: Radioelektronika, Kyiv, Ukraine)*, Allerton Press, Inc. New York, vol. 37, no. 11, pp. 23-26, 1994.

[26] R. S. Volodymyrovych, K. A. Pavlovych, and V. I. Andriiovych, "Research of the Sensitivity of the Quantized Coefficients of a Digital Bandpass Filter with Frequency Sampling," *Indonesian Journal of Electrical Engineering and Informatics (IJEEI)*, vol. 8, no. 1, pp. 74–82, Mar. 2020, doi: 10.11591/ijeei.v8i1.1552.

[27] J. Proakis and D. Manolakis, *Digital Signal Processing: Principles, Algorithms, and Applications*, 3rd ed. Upper Saddle River, NJ, USA: Prentice Hall, 1996.

[28] A. V. Oppenheim and R. W. Schafer, *Discrete-Time Signal Processing*, 2nd ed. Upper Saddle River, NJ, USA: Prentice Hall, 1999.

[29] S. K. Mitra, *Digital Signal Processing: A Computer-Based Approach*, 4th ed. New York, NY, USA: McGraw-Hill, 2011.

[30] R. Lyons, "2nd-order IIR resonators: A contradiction resolved," DSPRelated.com, 2018. [Online]. Available: https://www.dsprelated.com/showarticle/183.php. (Accessed: Jun. 6, 2025).

[31] V. Cappellini, A. G. Constantinides, and P. Emilliani, *Digital Filters and Their Applications*, London, U.K.: Academic Press, 1978.

[32] A. V. Oppenheim and R. W. Schafer, *Digital Signal Processing*. Englewood Cliffs, NJ, USA: Prentice-Hall, 1975.

[33] A. Antoniou, *Digital Filters: Analysis and Design*. New York, NY, USA: McGraw-Hill, 1979.

[34] H. L. F. Lam, *Analog and Digital Filters*. Englewood Cliffs, NJ, USA: Prentice-Hall, 1979.

[35] R. E. Bogner and A. G. Constantinides, Eds., *Introduction to Digital Filtering*. London, U.K.: John Wiley and Sons, 1975.

[36] E. C. Ifeachor and B. W. Jervis, *Digital Signal Processing: A Practical Approach*, 2nd ed. Harlow, U.K.: Addison Wesley, 2002.

[37] L. R. Rabiner and R. W. Schafer, "Recursive and nonrecursive realizations of digital filters designed by frequency sampling techniques," *IEEE Transactions on Audio and Electroacoustics*, vol. 19, no. 3, pp. 200-207, September 1971, doi: 10.1109/TAU.1971.1162185.
[38] L. R. Rabiner, "Techniques for designing finite-duration impulse-response digital filters," *IEEE Transactions on Communication Technology*, vol. 19, no. 2, pp. 188–195, Apr. 1971, doi: 10.1109/TCOM.1971.1090625.
[39] P. A. Stubberud and C. T. Leondes, "The design of frequency sampling filters," *in Control and Dynamic Systems, Vol. 68: Digital Signal Processing Systems: Implementation Techniques*, C. T. Leondes, Ed. San Diego, CA, USA: Academic Press, 1995, pp. 163–198.
[40] K. A. Rao, A. Kumar, S. K. Patel, D. Kaplun, and N. Purohit, "Design of frequency sampling rational rate polyphase FIR converter," *IEEE Transactions on Circuits and Systems II: Express Briefs*, vol. 71, no. 2, pp. 962-966, Feb. 2024, doi: 10.1109/TCSII.2023.3309843.
[41] C. M. Rader and B. Gold, "Digital filter design techniques in the frequency domain,"*IEEE Transactions on Electromagnetic Compatibility*, vol. EMC-10, no. 2, pp. 221-221, June 1968, doi: 10.1109/TEMC.1968.302949.

BIOGRAPHIES OF AUTHORS

Serhii Rybka received the degree of electrical wire communication engineer at the Kyiv Higher Military Engineering School of Communication in 1983. From 1983 to 1990, he worked as an engineer at fixed communication nodes. From 1990 to 2000, he was engaged in scientific and pedagogical activities at a higher educational institution. From 2000 to 2016, he worked as a manager of stateowned enterprises in the field of communication. In 2013, he obtained the scientific degree of Candidate of Technical Sciences. Currently, he is an advisor to the director of G.E. Pukhov Institute for Modelling in Energy Engineering. His scientific interests include the design of FSF and FSF banks, as well as Lagrange-structure filters. He can be contacted at email: ars09@ukr.net.

Ivan Varava received a Master's degree in Computer Science from the National Technical University of Ukraine "Kyiv Polytechnic Institute" in 2003. In 2017, he was awarded the degree of Candidate of Technical Sciences at the V.M. Glushkov Institute of Cybernetics of the National Academy of Sciences of Ukraine. He currently holds the position of Associate Professor in the Department of Software Engineering in Energy at the National Technical University of Ukraine "Igor Sikorsky Kyiv Polytechnic Institute." His scientific interests include data processing and computer simulation. He can be contacted at email: varava_ivan@lll.kpi.ua.